Small data problems in deep learning applications with remote sensing: A review

Anastasiia Safonova[1*], Gohar Ghazaryan[1], Stefan Stiller[1,2], Magdalena Main-Knorn[1], Claas Nendel[1,3] and Masahiro Ryo[1,2]

[1] Leibniz Centre for Agricultural Landscape Research (ZALF), Müncheberg, Germany

[2] Environment and Natural Sciences, Brandenburg University of Technology Cottbus-Senftenberg, Cottbus, Germany

[3] Institute of Biochemistry and Biology, University of Potsdam, Germany

Correspondence: anastasiia.safonova@zalf.de

Abstract

Researchers and engineers have increasingly used Deep Learning (DL) for a variety of Remote Sensing (RS) tasks. However, data from local observations or via ground truth is often quite limited for training DL models, especially when these models represent key socio-environmental problems, such as the monitoring of extreme, destructive climate events, biodiversity, and sudden changes in ecosystem states. Such cases, also known as *small data problems*, pose significant methodological challenges. This review summarises these challenges in the RS domain and the possibility of using emerging DL techniques to overcome them. We show that the small data problem is a common challenge across disciplines and scales that results in poor model generalisability and transferability, yet this has not been investigated in a structured way. We first introduce ten emerging DL techniques: transfer learning, self-supervised learning, semi-supervised learning, few-shot learning, zero-shot learning, active learning, weakly supervised learning, multitask learning, process-aware learning, and ensemble learning; we also include a validation technique known as spatial k-fold cross validation. These techniques have shown promising potential in other scientific disciplines, but have been rarely applied in the RS domain. We also provide guidance on which learning technique to use in various cases, which helps to create a more methodologically robust DL application (and a greater number of them) that can be used to tackle socially important problems with limited data.

Introduction

Over the last decade, Artificial Intelligence (AI) technologies, especially Machine Learning (ML) and Deep Learning (DL), have been increasingly used for understanding and predicting human-environment interactions[1]. ML is a subset of AI that implements algorithms which use data to learn how to perform a specific task without being explicitly programmed. DL is a subset of ML that focuses on training deep neural networks capable of implicit feature extraction from unstructured data, such as images, text, and

sound[2–4]. Scientists have actively employed DL for image processing and data analysis, recently providing innovative solutions in the field of Remote Sensing (RS) to detect and classify objects on Earth. This study defines RS as the use of satellite and aircraft-based sensors.

The expanding field of RS provides an abundance of data streams from numerous sources. This, combined with the growing array of available data products, delivers a wide range of data that is useful for addressing various problems. Among them, Landsat, has been operational since the early 1970s and provides a unique long-term record of satellite imagery with a 30-metre spatial resolution. The Copernicus programme's Sentinel-2 system generates data with a 10-metre spatial resolution, offering a balance between spatial detail and data continuity as well as radar imagery based on the Sentinel-1 mission. One recently launched hyperspectral mission, the Environmental Mapping and Analysis Program (EnMap), stands out with over 200 spectral bands and a 30-metre spatial resolution; this offers unique opportunities for researchers to map ecosystems and their changes in detail. In addition, commercial platforms, such as SkySat, provide extremely high-resolution data with a spatial resolution of less than one metre[5,6]. Together, these diverse RS platforms contribute to a more comprehensive understanding of the Earth's surface across different scales and domains[7]. For this reason, these RS products are widely used to study local and regional environmental problems, including agricultural productivity[8,9], the water quality of lakes and ponds[10], the ecological patterns of forests and grasslands[11], and damage to natural, cultivated, and inhabited land through extreme weather events. Since the spatial and temporal resolution of RS products is likely to continue increasing, DL applications are expected to become even more popular for solving fine-scale local issues where each local site has its own unique conditions and context[12–14].

Since DL algorithms have fewer inductive biases but larger parameter counts than conventional ML algorithms, DL models normally require a large amount of data for training[15–19]. DL methods usually learn from raw data and skip manual feature engineering steps; this means that human efforts are not needed to quantitatively measure some attributes from the data. For example, DL algorithms can learn from image data directly, instead of using the extracted shape and size of an object in an image. When sufficient data is available, DL methods can automatically extract the meaningful features from low to high levels for prediction[20]. However, although raw data of common events is generally abundant, the lack of sufficient labelling information makes the collection and preparation of a large reference dataset[21] a persistent challenge for many RS applications. Moreover, certain scenarios also lack available reference data. For instance, biodiversity monitoring needs a large number of human observers well trained in taxonomic classification, which often prevents observation campaigns from generating datasets large enough for sound DL applications. Furthermore, anomaly events such as climate extremes and disease outbreaks are too rare

for researchers to acquire sufficient data coverage. Their sample size is often as small as n = 1–300, which is usually insufficient for DL application [22].

The gap between the large data availability of RS imagery and the small data[23] availability of several important real-world environmental problems (referred to as the "small data problem") is a very common challenge. It is hard to acquire the ground-truth response labels associated with the input features. This makes sense, because the goal of most of these studies is to develop a model designed to predict a specific response variable from the various observed input features. However, traditional DL training methodologies require a large initial set of labelled data to train predictive models. It is increasingly clear that this is an emerging problem for AI, and researchers have proposed several novel DL techniques that require less labelled data (e.g., transfer learning and self-supervised learning). However, to the best of our knowledge, the small data problem has not been systematically tackled as an emerging scientific challenge in the RS domain.

In this review, we summarise the current research on the small data problem in RS (particularly as it relates to DL) and suggest promising DL techniques to address this problem. First, we explore how the small data problem can be defined. Second, we describe a few common elements of the previous studies. Third, we present the advantages and disadvantages of using a small dataset. Finally, we offer a set of practical recommendations about how RS scientists can better implement DL techniques to fully make use of a small dataset. We believe that the small data problem is a common – but still unsolved – issue for recent RS applications, and therefore, this review should serve as a valuable resource for supporting RS and DL applications in scientists' and policymakers' attempts to address a wide range of environmental problems.

What is the small data problem?

We argue that a dataset can be considered large (not small) when the dataset consists of >100,000 annotated samples, or when it covers the entire probability distribution in a high-dimensional space. In this case, model generalisability and transferability are expected to be high. For example, there are several free large datasets that can be used for DL: the ImageNet dataset, containing over 14 million annotated images[21], the Common Objects in Context (COCO) dataset, containing 330K images, 1.5 million object instances, and 80 object categories[24], and the OpenImages dataset, containing over 9 million images[25]. These datasets can be used for training a large DL model with thousands to millions of parameters. In the RS domain, land use / land cover classification would be a typical example.

In contrast, data is more likely to be regarded as small (or not large enough) when the dataset consists of <1,000 annotated samples, the dataset covers the distribution poorly, or the number of samples is expected to be insufficient when using DL to find meaningful features. This is a frequently occurring situation, but it can be a significant challenge for training deep neural networks[26,27]. A relatively small dataset can

negatively affect the performance of a DL model due to overfitting, which is when a model performs well with the training data but poorly on new, independent testing data. This therefore results in low levels of model generalisability and transferability. A common case within the RS domain (but particularly relevant) is that the data can be "extra-small", meaning that the dataset consists of just 1–10 annotated samples (e.g., historical natural disasters and disease outbreaks). The size would be sufficient for human beings to start guessing what features can uniquely describe the target, but it would not be sufficient for automated, implicit DL feature extraction.

In the DL domain, the Tiny ImageNet Dataset[28] (also known as MicroImageNet) contains 500 images for each class (of 200 classes), indicating that DL scientists regard this level of data size as small. According to the articles we reviewed in the following section, the majority of the studies targeted classification of a few types, and many of them collected less than 500 images for each class (e.g., refs.[29–45]).

There should not be a strict divide between "small" and "large" when training DL models, because the size of the dataset required may depend on various factors such as the complexity of the task and the number of features in the data. Typically, the challenges stemming from a limited amount of labelled data increase with system complexity, the rarity of observations (e.g., endangered biological species), and the coverage of geographic area. Also, classification and detection problems may need less data than regression problems. Nevertheless, a convincing theoretical argument for separating the two could be made based on whether a trained DL model exhibits a "double descent", which means that a model's performance initially improves with increased complexity, worsens, and then improves again, contradicting the traditional expectations of a bias-variance trade off (ref.[46]). When the dataset is not large enough, the model tends to remember all possible case-by-case instances without generalisation (and thus overfit). However, once the dataset is large enough, the DL model starts learning a handful of general features[47].

The small data problem may be relevant to the "small n, large p ($n<p$)" problem in statistics, where the sample size n is much smaller than the number of parameters p (also known as the "short, fat data" problem). As a rule of thumb, each parameter can be reasonably estimated with n = 5–10. According to this logic, it is then possible to estimate how many samples might be needed for a given DL model. Even one of the simplest convolutional neural network (CNN) architectures, LeNet-5 (two convolutional and three fully connected layers), still has about 60,000 parameters[48]. The most popular CNN architectures have 10 million to 100 million parameters (e.g., AlexNet, VGG, Inception, and ResNet)[49], and there is a trend towards increasing the number of parameters for achieving better performance (e.g., large language models). For instance, vision transformers[50] have recently gained more and more traction, with some models consisting of more than 20 *billion* parameters[51].

Deep learning applications in RS with the small data problem

This section is a literature review describing how common the small data problem is in the RS domain. Initially, we made a Web of Science Core Collection search with the following keyword combination in the "all fields" category: {"*remote sensing*" AND ("*deep learning*" OR "*convolutional neural*" OR "*recurrent neural*") AND ("*small data*" OR "*small sample*" OR "*limited sample*" OR "*limited data*")}. We found 161 articles as of 18 January 2023. We first examined all titles and abstracts, and discarded irrelevant articles. Moreover, we relied on snowball sampling of relevant papers from the reference lists of the literature that had not emerged via the systematic search but were relevant to the main goals of this review. This resulted in 80 additional articles. The list of articles with detailed information is available in Appendix A. Our approach may have omitted several articles that also addressed the small data problem, but the goal here was not to cover every single previous study. Instead, we have attempted to describe how broad the issue is, and such an effort may not be worthwhile, given the speed of scientific progress, where today's comprehensiveness may be far less important in the next couple of years.

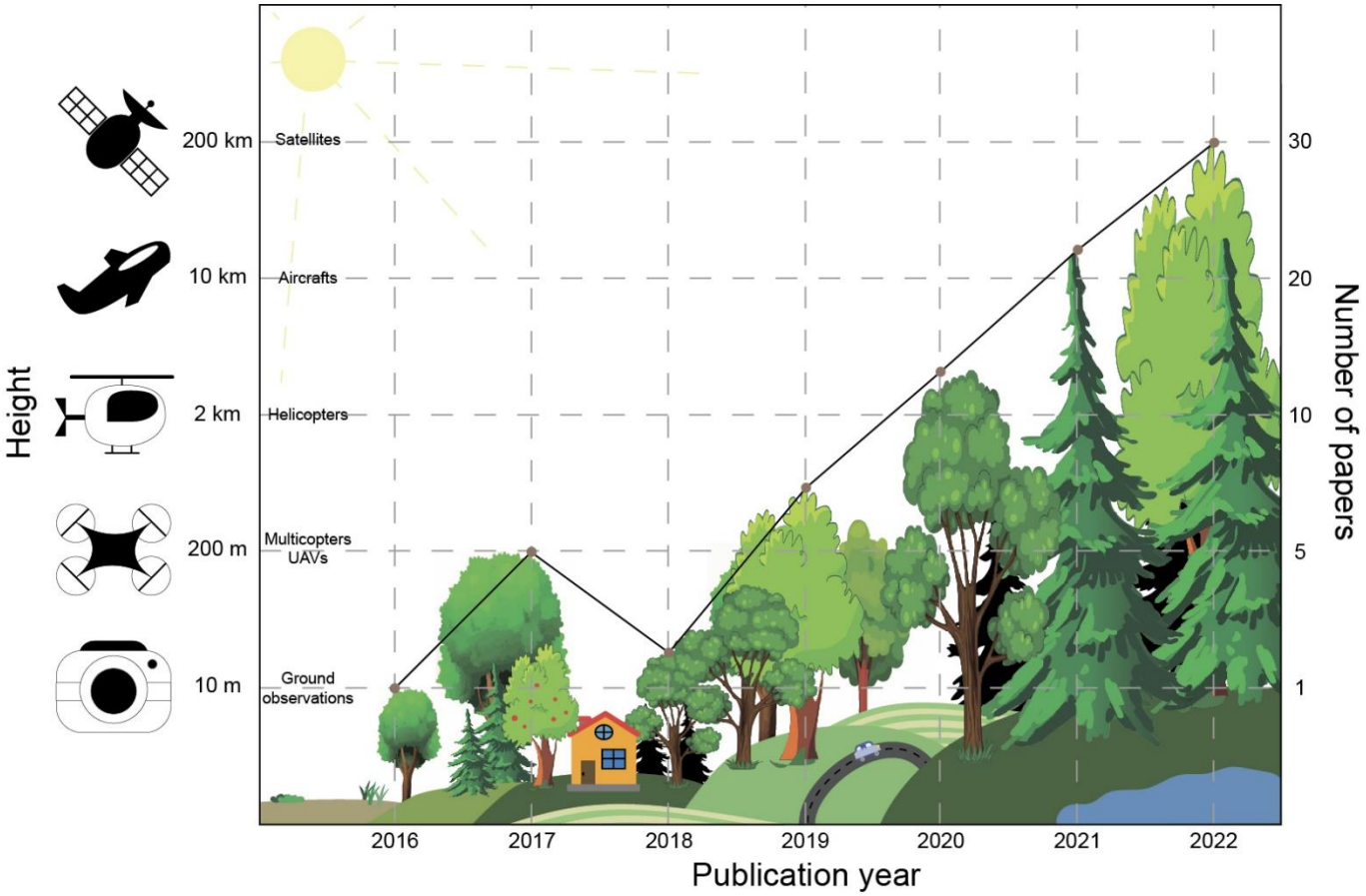

Figure 1. An overview of publication trends where studies use RS with a limited number of annotated data and DL (since 2016). The number of peer-reviewed papers per year and the maximum spatial coverage using RS techniques have been increasing over time. Most of the previous studies focused on vegetation monitoring.

As a general publication trend over time, we found that the number of papers, as well as the spatial extent of interest, have increased over the years; most papers were related to vegetation monitoring (Figure 1). In addition, we summarise and describe the reviewed publications in the following subsections based on five key findings:

(1) Various DL algorithms with various RS data sources have been used for a few common problems.

(2) The small data problem is a scale-dependent issue.

(3) Data augmentation and transfer learning are popular, but other techniques are rarely used.

(4) Reported model performances are suspiciously high, indicating a lack of appropriate evaluation schemes.

(5) Using a small dataset has several attractive benefits.

Various DL algorithms using different RS data sources are used for a few common problems

RS and DL have had a major impact in many areas, particularly in vegetation-related applications (49 of the 80 articles), followed by land use / land cover classification (16 articles), and vehicle detection or classification (5 articles). The majority of the studies conducted classification (44 articles), followed by segmentation (19 articles), and object detection (17 articles). The majority (86%) of the studies had 1,000 or fewer annotated samples per class (median: 242 samples per class; mean 616). Few studies addressed a regression problem, but this does not necessarily indicate a lack of research on RS and DL for regression. Rather, it suggests that such tasks are more complex and require larger labelled datasets, as evidenced by the reliance on larger amounts of labelled data in several published studies[52,53].

Vegetation-related applications included mapping crop type[54–56], as well as monitoring plant health[36,57–60] and predicting crop yields[43,61–63]. For instance, around 800 labelled data points were used for classification of crops using Sentinel-1 data[64], and around 300 field data points were used for yield estimation with Planet and WorldView data from 2D and 3D CNN[61]. In addition, RS has contributed to biodiversity conservation by its use in analysing complex ecosystems, tracking habitat changes, and identifying plant species. For example, Muro et al. (ref.[65]) used Sentinel-1 and -2 data in a DL model to predict plant biomass and species richness, using around 500 observations. Another example is a study by Lange et al. (ref.[54]), where CNNs were used to map grassland use intensity.

Besides vegetation studies employing global satellite data, various other RS sources have been used. For example, one study focused on mapping urban areas used in high-resolution satellite imagery to create detailed maps of buildings and infrastructure[55], while another study focused on monitoring changes in vegetation cover used in lower-resolution imagery from a different satellite sensor[66]. In addition, a study of land cover mapping used a combination of different data sources, including aerial imagery, LiDAR, and field data[67,68]. Hyperspectral RS, a technology that acquires high-dimensional spectral information across

hundreds of contiguous spectral bands, is another popular data source. However, obtaining manual annotations for hyperspectral data is challenging, leading to an insufficient number of labelled pixels[69,70]. While DL techniques may hold potential for hyperspectral image classification (e.g., Spectral MugNet), further research is required to explore their effectiveness in scenarios with limited data[71,72].

We also found that several studies used the same dataset repeatedly by using different DL algorithms. One series of studies[29,59,60,73–80] used the same hyperspectral images (HSIs) from a dataset held by the Italian University of Pavia. Some of these authors compared these HSIs with other available HSI datasets: Salinas – six papers (refs.[60,73,75,76,78,79]), Indian Pines – six papers (refs.[59,73,75–77,80]), Kennedy Space Center – two papers (refs.[74,77]), and Houston – two papers (refs.[59,60]).

Analysing the same dataset using different approaches is a reasonable way to confirm how well a new technique may perform in comparison to previous ones, but this repetition also indicates that similar investigations of various issues is still challenging, probably due to the small data problem. Nevertheless, we found that a few studies have investigated the monitoring of extreme events, including natural fire occurrences[81,82] and algal bloom events[83]. We expect future studies to address other equally important global change events, such as conflicts, energy issues, and biodiversity problems.

The small data problem is a scale-dependent issue

The importance of spatial resolution and spatial extent in RS data is another factor that directly influences the level of detail captured and the subsequent insights that can be derived from the imagery[84,85]. The small data problem becomes more pronounced when analysing high-resolution data, such as data obtained from Unmanned Aerial Vehicles (UAVs), which can offer centimetre-level granularity. This is because the fine-scale details captured in high-resolution imagery increase the variability and heterogeneity of the landscape, making it more difficult to generalise from a limited set of labelled examples. In contrast, satellite data with spatial resolution generally in the range of a few metres have different challenges related to labelled data. This relative lack of resolution can reduce the variability of the terrain, and oversimplify the representation of features in the imagery.

Different sources of data also exhibit different advantages and disadvantages related to their spatial extent. Satellite data typically covers a much larger area compared to UAV data. The spatial predictions generated from satellite data can be reliable across vast regions if there is an adequate number of labelled samples and if their spatial distribution is representative of the entire area of interest (e.g., geographically isolated areas). The distribution of labelled data plays a critical role in the performance and generalisation capabilities of DL models trained on RS data. In contrast, when working with high-resolution UAV data, the focus is more on capturing the fine-scale details and variations within a smaller area of interest. In this context, the challenge lies in accurate local measurements that reveal subtle differences.

Data augmentation and transfer learning are popular, while other techniques are rarely used

Data augmentation and transfer learning (TL) have become very common ways to improve models when applying DL techniques to RS data under conditions of small data. Our review found that 71% of all studies employed some sort of data augmentationtechnique[86] while TL was present in 14 works (for example, see refs. [42,87,88]). Data augmentation is a technique to artificially expand a dataset by creating new samples through various transformations, such as rotation, scaling, and flipping, to improve a model's generalisability and robustness. Transfer learning is a technique where a pre-trained model, often on a large-scale dataset, is fine-tuned for a different but related task or dataset, leveraging the previously learned features to improve generalisability.

Various data augmentation techniques were used in most of the papers included in this review. The choice of data augmentation technique depends on the quantity, quality, and type of RS data. Most commonly, this method was applied to limited data from satellite imagery obtained from Landsat, WorldView, extremely high-resolution imagery, images from UAVs, and others. The most common methods of increasing RS data were: manual or automatic cropping of a large image or orthophoto image into small patches ranging from 15 × 15 pixels to 250 × 250 pixels or more, geometric image transformations (resizing, cropping, rotation, horizontal reflection, etc.), and colour transformations (changing contrast, brightness, colour, applying various noise filters, etc.). Nevertheless, as we show in the practical recommendation section, other DL techniques exist, but they are still rarely used.

Reported model performances are suspiciously high

While it was challenging to compare the studies under review in terms of model performance because they reported different metrics, we found an interesting but potentially problematic trend throughout the previous works. In essence, many studies tended to report an overoptimistic, overfit result, without testing model generalisability and transferability.

One of the most popular metrics was *Accuracy* (59 papers). The following evaluation metrics were also frequently used: *Precision* (P) in 39 papers, *Recall* (R) in 30 papers, *F1 score* (F1) in 28 papers, *Kappa coefficient* (k) in 16 papers, *Intersection over Union* (IoU) in 13 papers, *mean Average Precision* (mAP) in 10 papers, *Sensitivity* (S) in 3 papers, *p-value* by Freeman et al. (ref.[30]), *Root Mean Squared Error* by Wang et al. (ref.[89]) and Hong-Yu et al. (ref.[31]), *Mean Absolute Percentage Error* by Barbosa et al. (ref.[90]), and *Dice Similarity Coefficient* by Khan et al. (ref.[91]). Most papers used metric combinations (55 articles, 68%). We found that the reported performance was extremely high. In 32 of the 59 articles reporting "Accuracy", the score was 95% or more. Accuracy of 99-100% was achieved in 11 studies. Measurements of "Precision" were higher than 0.98 in some studies. The F1 metric was 90 or higher in at least 14 of the 28

papers. Some studies reported even 100% accuracy or an F1 metric of 100, which is a clear sign of overfitting. The tendency of these outstandingly high scores might result from the model evaluation scheme. Typically, the test dataset should be collected independently from the data collection used for model training and validation, and the model performance should be evaluated using the test dataset. Otherwise, the model test was done for the same, biased dataset, e.g., the test was not done in another region, spatial autocorrelation was ignored, or the test was not done with data from other years. As a result, the models are neither generalisable nor scalable, but highly specialised for the particular data acquisition pipeline. Also, it is possible that augmented data was used in both training and test datasets. In the practical recommendation section, we suggest some promising solutions – cross validation in particular – to these problems.

Using a small dataset has several attractive benefits

It is often the case that it is impossible to obtain additional annotated data regardless of whether the researcher wants it or not: these include, for instance, studies that investigate rarely observed phenomena (e.g., climate extremes, rare species, and disease outbreaks), cover a specific narrow geographic space (e.g., a single agricultural field), are limited by time and resources (e.g., studies in low-income countries), or those that employ data recorded before digitalisation. However, this does not mean there are no advantages of using a small dataset to solve various RS problems by using DL.

One of the biggest advantages of using a small RS dataset is faster training times. This can be particularly useful for prototyping and experimentation with different models and hyperparameters. With smaller datasets, multiple models can be trained in a relatively short time, making it easier to compare and select the best model[92,93]. Another benefit is reduced memory requirements and less storage. The use of a smaller dataset reduces the memory requirements, making it possible to train on resource-constrained devices, such as laptops or embedded systems[94]. A small dataset may also make it difficult to train (overly) complex models with many parameters. In these cases, simpler models may indeed be more suitable; they also have the advantage of being easier to train and validate the performance of the model[95–98]. The use of a small dataset combined with a low-complexity model can still result in sufficient performance[23]. Collecting and labelling an RS dataset is in some cases a complex, time-consuming, and costly task for research centres and organisations, which often leads to the use and preparation of a small set of available data. It could be drone data, digital camera imagery, or a few plots of satellite data. Thus, the use of a small dataset can reduce operating costs[99,100]. Finally, small datasets are easier to annotate, which is useful in cases where manual annotation is required.

Of course, small datasets have downsides as well. The main disadvantage is the lack of generalisability and transferability due to overfitting[101], resulting in poor performance when using unforeseen datasets[102–104].

Small datasets also may be biased[92,105,106].

Practical recommendations for DL implementation strategies

In the previous section, we noted that data augmentation and transfer learning are popular, but other techniques are rarely used. To address this issue, this section offers practical recommendations on strategies for the implementation of DL. We introduce the following techniques: TL, self-supervised learning, semi-supervised learning, few-shot learning, zero-shot learning, weakly supervised learning, process-aware learning, multitask learning, and ensemble learning. The literature search in this section was conducted in the same way as the previous search for major issues. However, we added a query that was able to return studies applying one of the above-mentioned techniques (e.g., "transfer learning", "semi-supervised learning", "few-shot learning") to the main search keywords. We found 32 articles as of 16 February 2023 (Figure 2). We also present a practical flowchart for deciding which algorithm to use in each specific use case (Figure 3). We do not explicitly cover other methods such data augmentation and regularisation, since they have been widely covered in various literature, such as by the work by Shorten and Khoshgoftaar[86].

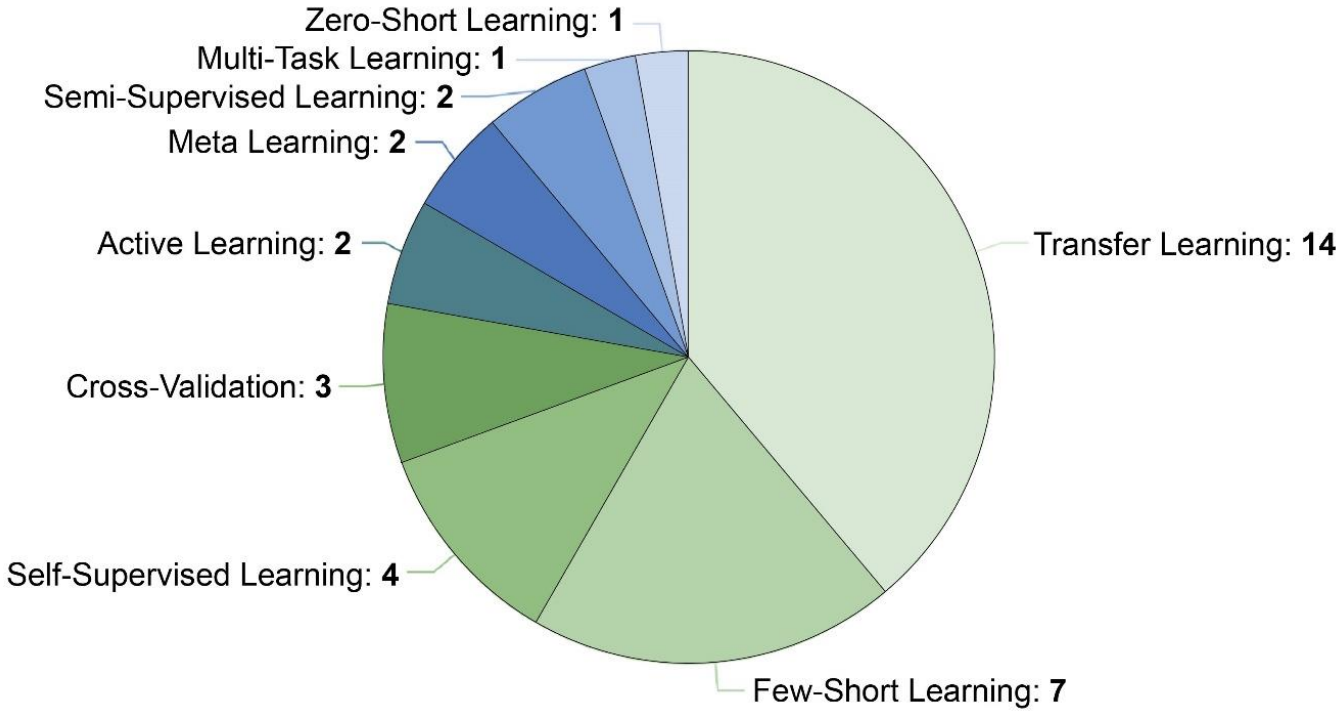

Figure 2. The number of articles that use particular DL techniques addressing the small data problem in RS applications as of February 2023.

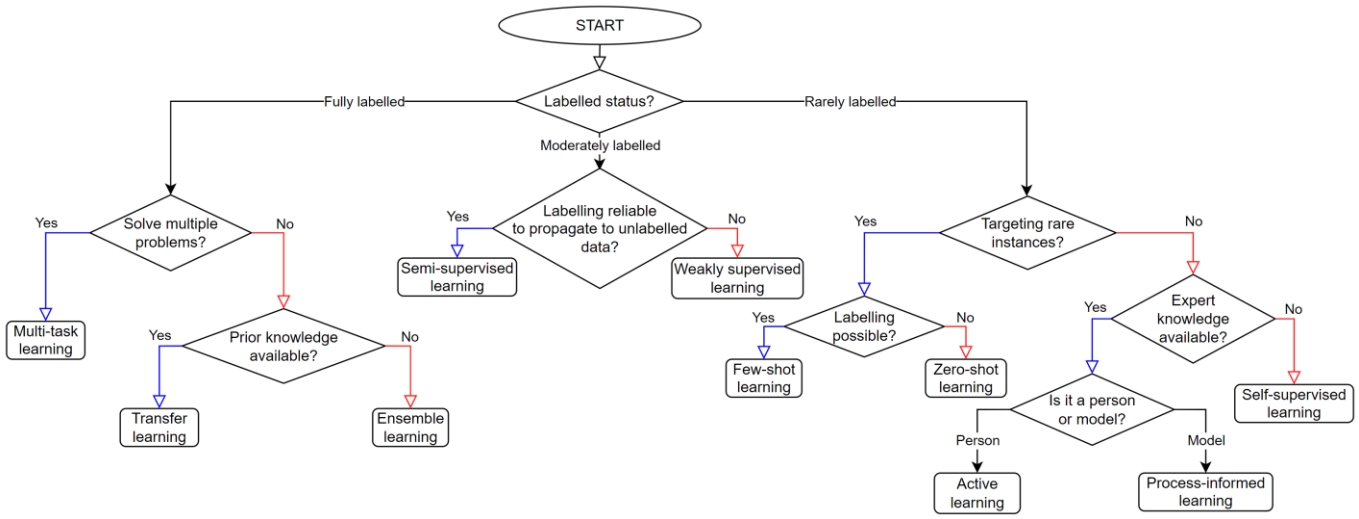

Figure 3. Practical flowchart for selecting an appropriate deep learning technique (as of May 2023) to address the small data problem in remote sensing applications.

Transfer learning

As described before, TL is a popular technique that derives learning from one task and reuses it to solve another (similar) task. As Iman et al. have explained[107] TL is widely used in labelled dataset fields such as radar images, medical images, malware classification, facial emotion recognition, mechanics, vision, human activity recognition, civil engineering, Natural Language Processing (NLP), military, human sciences/psychology, chemistry, security, physics/astrophysics, and telecommunications.

Typically, TL takes place when a neural network is pre-trained on a large dataset, such as ImageNet[21], and then its weights are used to fine-tune it on a smaller dataset for a specific task. TL can also be used as a feature extraction method to develop a second model that can be trained on the target data. The idea of TL is to apply knowledge from the source task to the target task, potentially improving performance, reducing the need for large training data, preventing overfitting, reducing the otherwise huge computation cost, and saving time[108]. Pre-training on a general dataset is particularly effective when the task-specific dataset is small or when there is limited labelled data available.

We found three ways that TL was used in the literature: fine-tuning a pre-trained model, using pre-trained features as input for a new model, and combining pre-trained models. Fine-tuning involves taking a pre-trained model and training it further on the target task[109,110]. Using pre-trained features means that the output of one or more layers of a previously trained model is used to develop a new model trained on the target task. Combining pre-trained models involves training multiple pre-trained models on related tasks and then subsequently combining them to make predictions about a different, previously unexplored phenomenon.

TL is already actively used to solve a variety of problems in RS when the dataset is small. We found a total of 14 papers regarding the use of TL in RS on a small sample. For example, a paper by Wang et al.[111] proposed a DL framework for RS image registration based on TL that would reduce the huge computational

cost in the training stage, speed up the framework, and achieve additional performance gains. The experiments conducted on seven sets of RS images acquired by RADARSAT, SPOT, and Landsat showed that the proposal improved registration accuracy by between 2.4% and 53.7%.

Zhang et al.[112] used TL to classify HSI due to very limited training data and the massive parameters of end-to-end 3-D lightweight models. Moving to the problem of radar-jamming detection, Hou et al. (ref.[113]) and Lv et al. (ref.[114]) separately proposed methods based on TL. In Character et al. (ref.[115]), researchers used TL not only to compensate for a small dataset (Lidar and Sonar), but also to address false positives by training the YOLOv3 model on both shipwrecks and background topography. Another example was forest-fire detection using YOLOv5 by Xue et al. (ref.[82]), improving the performance of mAP@0.5 by up to 10.1%. Wang et al. (ref.[116]) applied TL to weed density extraction based on few-shot learning through UAV and multispectral images in an ecological irrigation area using a pre-trained AlexNet algorithm.

A kind of TL known as domain adaptation was applied to synthesise training data under diverse environmental conditions with automatic labels using YOLOv3 (ref.[117]). The results from that paper showed that their proposed method improved bale detection. Moreover, this approach could be easily scaled to many other crop field objects. Chen et al. (ref.[118]) used the Faster R-CNN domain adaptation for aircraft detection on the DOTA dataset. Yu et al. (ref.[88]) showed that their method based on TL could accurately extract terraced field surfaces and segment terraced field boundaries with an overall accuracy above 93.12%.

In another experiment, TL solved the problem of poor adaptability of the DenseNet-121 network to RS images acquired from different platforms, and was able to properly identify disaster-damaged buildings[119]. Other examples included scattering shrub detection[42], fir tree detection[36], HSI classification[59], land cover classification[120,121], and seismic data analysis[122]. The average accuracy in these works after applying TL to the new small datasets was over 93%.

Key recommendations for using TL include selecting the right pre-trained model, determining the level of TL (feature extraction, fine tuning, or both), determining which layer(s) to transfer, generously employing data augmentation, regularising the network, and evaluating performance. One common practice is to import and use ready-made models from DL libraries such as TensorFlow, Keras, Theano, and PyTorch. The most popular models were AlexNet, VGG, Xception, Inception, MobileNet, DenseNet, ResNet, GoogleLeNet, and YOLOs. Abu et al. (ref.[123]), Sharma et al. (ref.[124]), and Zhao (ref.[100]) all suggested considering fine-tuning several hyperparameters (feature map, filter size, activation function, pool size, optimiser, learning rate, batch size, epoch, dropout rate, loss function, and evaluation metric) of the pre-trained model.

Self-supervised learning

Self-supervised learning is a technique related to transfer learning. However, in contrast to traditional transfer learning, self-supervised learning does not require labelled data for pre-training – it can leverage the structure of unlabelled data to generate labels for the pre-training task. However, like transfer learning, a model pre-trained with self-supervised learning is further fine-tuned on the labelled downstream task[125]. This technique has been employed in medicine and healthcare[126,127], physics[128], speech representation[129], RS[116], time-series analysis[130], video processing[131–133], speech processing[134], and target tracking[135] for example. The most-cited papers involve medical research, solving problems such as accurate detection of tissue in monocular endoscopy[136], retinal disease diagnosis[137], MRI parameter mapping or reconstructio[138,139], 3D medical-image analysis[140], and homography estimation[141].

However, we only found four papers dealing with self-supervised learning in RS using a small sample[60,142–144]. These were related to solving the HSI classification problem. The main reason for using self-supervised learning was the scarcity and high cost of labelled HSI samples. In Song et al. (ref.[144]), the authors proposed a dual-branch residual neural network (ResNet) to fuse spectral and spatial information. Xue et al. (ref.[60]) proposed a generative self-supervised feature learning architecture for multimodal RS-imaged land cover classification. In this case, the self-supervised feature learning architecture was able to extract highly sophisticated, robust feature representations from multi-view data; this process did not require any labelled information, thus alleviating the otherwise critical need for annotated samples. To solve the same problem, Liu et al. (ref.[142]) presented a novel ensemble self-supervised feature learning method using multiple HSI datasets. Rangnekar et al. (ref.[143]) compared the performance of SegNet, U-Net, and Res-U-Net for scene understanding and object identification by using dense semantic segmentation to establish a benchmark for a given scene.

Despite the fact that the use of self-supervised learning technology on small datasets is relatively unexplored, we have come across some works on similar topics[145,146]. Su et al. (ref.[146]) presented a systematic study by varying the degree of domain shift and analysing the performance of multiple meta-learners on a variety of domains. The authors found that the improvements were greater when the training set was smaller or the task was more challenging. They also noted that self-supervised learning can degrade performance if the distributions of the images used for meta-learning and self-supervised learning are different. Cao and Wu (ref.[145]) proposed a system of scaled-down self-supervised learning, which included three parts: small resolution, small architecture, and small data. The authors showed that this approach could achieve impressive results on small data alone, even without a large pre-training dataset.

Semi-supervised learning

Semi-supervised learning is a technique that has been actively implemented in a number of different areas over the past few years. Self-supervised learning is a mix of supervised learning and unsupervised learning

to leverage unlabelled data, in which a model is repeatedly trained and updated using both the labelled and the generated pseudo-labels (that is, predicted labels) for the unlabelled data. This can result in better performance than supervised learning alone[147,148].

Across all scientific disciplines, one of the most-cited papers was presented by Ma et al. (ref.[149]) dealing with probabilistic representation and the inverse design of metamaterials. Another work was dedicated to detecting fake users on Twitter[150]. Later, Xu et al. (ref.[151]) presented a paper on image recognition and facial attribute recognition using a semi-supervised, self-growing generative adversarial network (SGGAN). The authors claimed that when they used training data with only 4% labelled facial features, their approach was nevertheless able to achieve accuracy comparable to that of leading supervised DL methods with all labelled facial features. Rostami et al. (ref.[152]) used semi-supervised learning to choose a subset of available features that had the lowest redundancy with each other but also the highest relevancy to the target class with limited training data in a Synthetic Aperture Radar (SAR) classification. Tseng et al. (ref.[153]) proposed DNetUnet for medical image segmentation. As of 2022, some of the most cited papers investigated road damage detection[154], drift compensation for olfactory sensors[155], and mechanical fault diagnosis[156].

As for the implementation of the semi-supervised learning strategy in the field of RS under conditions of small sample sizes, we came across only two articles. Jozdani et al. (ref.[157]) deployed a teacher-student semi-supervised learning approach (based on the U-Net and U-Net++ networks) involving unlabelled UAV and WorldView-2 data to assist with improving model performance to map caribou lichen. This approach produced a reasonably accurate (overall accuracy of 85% and F1 score of 84%) lichen map at the WorldView scale.

Although semi-supervised learning is suitable for unlabelled data, it is recommended to use labelled data because the quality of the labelled dataset will directly affect model performance. Another important point is to experiment with different ratios of labelled and unlabelled data to find the optimal balance for a particular task[158,159].

Few-shot learning

The goal of few-shot learning is to teach models to generalise for new tasks or problems with only a few labelled examples per class. Few-shot learning is therefore a type of meta-learning, which involves training a model on a set of related tasks so that the model can then learn to quickly adapt to new, similar tasks with only a few examples[160]. This method has gained popularity in RS for its ability to solve the problems of agriculture and areal scene classification[161,162]. Recently, Gao et al. (ref.[79]), Zuo et al. (ref.[163]), and Li et al. (ref.[164]) all applied meta-learning to HSI classification. Another approach is to use a widely cited generative adversarial network to teach the model a high-level representation of the data[165]. Despite the widespread popularity of such methods in the field of medicine[166], they are only recently beginning to be used in RS[167–

[169].

The application of few-shot learning in RS was found in seven articles in our search: Bai et al. (ref.[170]), Liu et al. (ref.[164]), Liu et al. (ref.[171]), Rao et al. (ref.[172]), Zuo et al. (ref.[163]), Wang et al. (ref.[116]), and Wang et al. (ref.[173]), and other. Most of the papers dealt with HSI classification problems. Wang et al. (ref.[116]) proposed weed and crop density extraction using RGB and multispectral images in an ecological irrigation area. Liu et al. (ref.[174]) proposed an algorithm based on few-shot learning in three steps. First, spectral-spatial features are extracted to reduce the labelling uncertainty via a deep residual 3-D CNN. Second, the network is trained in episodes to learn about a metric space where samples from the same class are close and those from different classes are far. Finally, the testing samples are classified by a nearest neighbour classifier in the learned metric space. A similar algorithm was also proposed by Bai et al. (ref.[170]). A small-scale high-precision network called "3-D convolution random Fourier features (3-DCRFF)" was presented by Wang et al. (ref.[173]). Yet another method was based on an edge-labelling graph neural network (FSL-EGNN) created by Zao et al. (ref.[163]).

Zero-shot learning

Zero-shot learning is a special type of few-shot learning method, which is trained to recognise objects or classes it has never seen before. The model is trained on a set of known classes or objects, but is also given additional information about the relationships between these classes, such as semantic or visual similarities[175]. This additional information is used to help the model recognise new, unseen classes or objects that are related to the known classes. This method is useful in situations where it is difficult or expensive to obtain labelled data for new classes or objects. The method has been applied to medical image segmentation[176], attribute-based classification[177], industrial fault diagnosis[156], and label-embedding for image classification[178]. We found only one article in RS applications, by Sumbul et al. (ref.[179]). Their paper presented object recognition for 40 different types of street trees using areal data. Experiments showed that their proposed model achieved a 14.3% normalised recognition accuracy for the classes with no training examples, which was significantly better than a random guess accuracy of 6.3% for 16 test classes, as well as the accuracy levels of three other zero-shot learning algorithms.

Both few-shot and zero-shot learning methods can be a valuable technique for extracting the best performance from limited data[112,180]. However, when using them with small samples, special attention should be paid to data augmentation, the selection of an appropriate evaluation metric, and the ensemble of multiple few-shot learning models. All of these can significantly improve the performance of the model.

Active learning

Active learning is a powerful technique that can help ML models achieve greater accuracy, while reducing

the amount of labelled data required[181,182]. This technique involves selecting the most informative examples, labelling them, and adding them to the training dataset. Active learning has been successfully applied in many disciplines, including NLP[183,184] and computer vision[185,186]. The idea of active learning use in RS in particular has been presented by Liu et al. (ref.[187]) and Cao et al. (ref.[188]) for HSI image classification. Some of the benefits of active learning include reduced labelling costs, faster training, and improved accuracy compared to randomly selecting examples for labelling. Active learning can be especially useful for small datasets, as it allows the model to learn more efficiently from a limited number of labelled examples. However, due to this data limitation, the model may be more prone to overfitting. To avoid this, we recommend applying regularisation methods and monitoring the performance of the model during training.

Weakly supervised learning

In cases when collecting full ground-truth labels is time-consuming, expensive, or otherwise practically impossible, then it is useful to use weakly supervised learning[189]. This is a type of ML in which the training data has been labelled partially, noisily, or imprecisely. One popular application of this is label propagation: the use of a small set of labelled data to generate labels for a larger set of unlabelled data. Another application is multi-instance learning, where each point of the training data exists in multiple instances, but a subset of these instances are labelled.

Weakly supervised learning has been successfully applied in various applications, including image classification, object detection, semantic segmentation, and NLP. However, the use of weakly supervised learning under the conditions of a limited dataset has only been presented in a small number of papers. In one striking case, Liu et al. (ref.[190]) presented an application that could identify acute lymphoblastic leukaemia with outstanding accuracy, approximately 91.9%. Another example was the classification of tiny spike-like projections on the basement membrane of the glomerulus by Wu et al. (ref.[191]). According to the results of the trial, the accuracy was 94.05%. Ruan et al. (ref.[192]) conducted two fault diagnosis experiments on ball bearings and bevel gears with 97.23% and 99.76% accuracy. Another example is a work presented by Kim et al. (ref.[62]) with segmentation for an autonomous combine harvester. Their results showed that their proposed weakly supervised crop area segmentation (WSCAS) method could be performed with the lowest inference time, and crop area could be localised with an IoU of about 94%. In all experiments, the authors of these papers claim that their proposed algorithms are superior to other existing methods, even under the conditions of a small sample size. It should be noted that we did not come across works where the methodology was used for RS on a small dataset. However, this technology has been actively used for optical images[193,194], areal and satellite images[195], and HSI[196].

Weakly supervised learning has the potential to reduce the cost and effort of collecting labelled data, and

can be used in various applications where obtaining fully labelled data is difficult or impractical, even in small datasets. One common approach is to use transfer learning and active learning, which can help improve model performance. In addition, using the weakly supervised learning method with limited data can help reduce the need for large amounts of labelled data, while still achieving high accuracy.

Multi-task learning

Multi-task learning is another powerful technique that can be implemented in RS when only a small dataset is available. It is designed to improve the performance of multiple related learning tasks by leveraging useful information among them[197]. The goal is to develop a model that can learn to generalise well about new instances of each task, while also benefiting from the shared knowledge learned across all tasks. This means that the model learns to solve multiple related problems using the same or shared representations, instead of developing independent models for each task. The model typically shares lower-level layers across all tasks, while having task-specific layers at higher levels. This way, the model can extract general key features shared across multiple tasks.

Multi-task learning's impressive track record has helped it gain popularity in recent years. The frequency of publications describing the use of this technology is growing by 25-30% every year. It has led to success in many ML applications, from NLP and speech recognition to computer vision and drug discovery[198–200]. Multi-task learning is also actively used in RS, particularly for classification[201], target detection[202,203], semantic segmentation[204,205], and feature representation tasks[206]. However, its application when using a small number of training samples is still rare, as only a single paper by Zhao et al. has discussed this[207]. Their paper proposed a multi-aspect SAR target recognition method based on a prototypical network. This method can significantly improve the recognition performance of the DL model under a small number of samples, and thus the recognition accuracy can approach that of a model with a complete training set.

Ensemble deep learning

Ensemble learning is a method that combines many individual models to obtain better generalisation performance (e.g., random forests and boosting). While this approach is commonly used for tabular data analysis, its application in DL models is far less popular because it requires huge computational resources and time. Nevertheless, ensemble DL models have the potential to harness the benefits of DL architecture as well as ensemble learning (e.g., to avoid overfitting). Previously, this method has been applied to predicting short-term traffic flow[208], predicting plant miRNA–lncRNA[209], and identifying the drivers of vehicles by using Controller Area Network (CAN) bus data[210]. Ganaie et al. also reviewed a variety of techniques that have been applied in different domains[211]. Liu et al. (ref.[142]) presented a novel ensemble self-supervised feature learning method on multiple HSI datasets. Since any of the above-mentioned

learning techniques can be combined, ensemble learning has promising potential for further applications.

Process-aware learning

Process-aware learning refers to the process of incorporating knowledge into ML models about the underlying processes or mechanisms that generate data. It is particularly helpful for understanding the underlying causal relationships between variables, thus leading to better predictions and decisions. One popular application is known as "physics-informed learning"(ref. [212]) in the domain of physics. Although we did not find the process-aware learning approach in any RS domain, we can imagine several use cases. For instance, researchers could use a vegetation growth model to simulate parameters that are difficult to measure in the field, use these simulated parameters as labelling for images, and then train a DL model with the labelled data.

Practical recommendations for DL model selection and validation strategies

As we mentioned above, it seems that previously reported model performances have been suspiciously high, indicating a lack of appropriate evaluation systems. Applying an appropriate validation strategy is important for model generalisability and transferability[213], while preventing overfitting[214].

The most commonly used type of validation strategy in ML is cross-validation[215]. This procedure is quite common in ML via tabular dataset analysis, but it is rarely applied to large datasets for DL. We believe that k-fold cross-validation would be useful for evaluating DL model performance with a small dataset – and this capacity for validation is another benefit of using a small dataset. Moreover, in the area of RS, random sampling for validation may not be the best idea, because spatial and temporal data typically reveal high autocorrelation levels. Several recent studies have pointed out that autocorrelation leads to a violation of the assumption of data independence between training data and the validation set[216–218]. Spatial rather than random cross-validation can be used for less biased model assessments[219].

The cross-validation technique was used by Xue et al. (ref.[220]) and by Chen et al. (ref.[221]) to solve problems with estimating PM2.5 concentrations across China, and by Yang et al. (ref.[222]) to estimate grassland biomass. Other case studies have included mapping soil properties from high-resolution RS data[223], mapping fire intensity[224], and quantifying rangelands[225]. We found four papers that directly investigated cross-validation for RS imagery under small sample conditions[30,54,56,226]. All the publications applied random cross-validation with different fold sizes (4 and 10 folds), each at different scales (local, regional, and national). The tasks performed were the mapping of regressed soil organic carbon content, HSI-based land cover classification, and plant water stress detection.

Conclusions

In this review paper, we performed a survey of the small data problem in RS data in DL implementation and suggested promising DL techniques to address the problem. First, we summarised 80 studies from 2016 to 2023, and presented the possibilities to address the small data problem with advanced DL techniques beyond conventional learning methods. For this, we first had to define what "small data" means. Then, we described the few previous studies that had analysed RS processes employing DL techniques under conditions of small data, and we looked at the advantages and disadvantages of using small datasets. Finally, we offered a set of practical recommendations about how RS scientists can better implement DL techniques to fully take advantage of a small dataset. As one previous paper noted[227] a variety of approaches can be used to solve the small data problem, such as data augmentation, data fine-tuning, the adaptation of pre-trained models, and reducing the dependence on large-sample learning. However, in our review, we also presented even more techniques that are worth considering when working with a small dataset. We identified a total of ten learning techniques for addressing the small data problem: Transfer learning, self-supervised learning, semi-supervised learning, few-shot/zero-shot learning, active learning, weakly supervised learning, multitask learning, ensemble learning, and process-aware learning. Cross-validation is also a valuable tool for improving the use of DL in RS (Figure 3). Our goal has been to show ways to implement DL applications for research where ground-truth (annotation) data is difficult to obtain, while making it possible to solve various problems involving classification, detection, or segmentation. These problems could include biodiversity loss, climate extremes, and sudden changes in socio-environmental systems. For future work, we plan to apply different DL strategies to solve various practical problems in RS under small dataset conditions, where this modern technique has not been adequately used. Finally, we hope that by justifying the use of small datasets, this review will motivate more researchers to experiment with other techniques and apply them to different RS problems.

References

1. LeCun, Y., Bengio, Y. & Hinton, G. Deep learning. *Nature* **521**, 436–444 (2015).
2. Chai, J., Zeng, H., Li, A. & Ngai, E. W. T. Deep learning in computer vision: A critical review of emerging techniques and application scenarios. *Machine Learning with Applications* **6**, 100134 (2021).
3. Lauriola, I., Lavelli, A. & Aiolli, F. An introduction to Deep Learning in Natural Language Processing: Models, techniques, and tools. *Neurocomputing* **470**, 443–456 (2022).
4. Sztahó, D., Szaszák, G. & Beke, A. Deep Learning Methods in Speaker Recognition: A Review. *Periodica Polytechnica Electrical Engineering and Computer Science* **65**, 310–328 (2021).

5. Murthy, K. *et al.* SkySat-1: very high-resolution imagery from a small satellite. in *Sensors, Systems, and Next-Generation Satellites XVIII* vol. 9241 367–378 (SPIE, 2014).
6. Fruth, T., Lenzen, C., Gross, E. & Mrowka, F. The EnMAP Mission Planning System. in *2018 SpaceOps Conference* (American Institute of Aeronautics and Astronautics, 2018). doi:10.2514/6.2018-2525.
7. Spoto, F. *et al.* Overview Of Sentinel-2. in *2012 IEEE International Geoscience and Remote Sensing Symposium* 1707–1710 (2012). doi:10.1109/IGARSS.2012.6351195.
8. Sawada, Y., Koike, T., Ikoma, E. & Kitsuregawa, M. Monitoring and Predicting Agricultural Droughts for a Water-Limited Subcontinental Region by Integrating a Land Surface Model and Microwave Remote Sensing. *IEEE Transactions on Geoscience and Remote Sensing* **58**, 14–33 (2020).
9. Taiwo, B. E. *et al.* Monitoring and predicting the influences of land use/land cover change on cropland characteristics and drought severity using remote sensing techniques. *Environmental and Sustainability Indicators* **18**, 100248 (2023).
10. Bhateria, R. & Jain, D. Water quality assessment of lake water: a review. *Sustain. Water Resour. Manag.* **2**, 161–173 (2016).
11. Zhu, X. *et al.* Grassland Ecosystem Progress: A Review and Bibliometric Analysis Based on Research Publication over the Last Three Decades. *Agronomy* **13**, 614 (2023).
12. Bai, T. *et al.* Deep learning for change detection in remote sensing: a review. *Geo-spatial Information Science* **0**, 1–27 (2022).
13. Kattenborn, T., Leitloff, J., Schiefer, F. & Hinz, S. Review on Convolutional Neural Networks (CNN) in vegetation remote sensing. *ISPRS Journal of Photogrammetry and Remote Sensing* **173**, 24–49 (2021).
14. Ma, L. *et al.* Deep learning in remote sensing applications: A meta-analysis and review. *ISPRS Journal of Photogrammetry and Remote Sensing* **152**, 166–177 (2019).

15. Fang, Y. *et al.* The impact of training sample size on deep learning-based organ auto-segmentation for head-and-neck patients. *Phys. Med. Biol.* **66**, 185012 (2021).
16. Adugna, T., Xu, W. & Fan, J. Comparison of Random Forest and Support Vector Machine Classifiers for Regional Land Cover Mapping Using Coarse Resolution FY-3C Images. *Remote Sensing* **14**, 574 (2022).
17. Akar, Ö. & Güngör, O. Classification of multispectral images using Random Forest algorithm. *J Geod Geoinf* **1**, 105–112 (2012).
18. Sharma, A., Ghosh, A. & Joshi, P. K. Decision tree approach for classification of remotely sensed satellite data using open source support. *J Earth Syst Sci* **122**, 1237–1247 (2013).
19. Thanh Noi, P. & Kappas, M. Comparison of Random Forest, k-Nearest Neighbor, and Support Vector Machine Classifiers for Land Cover Classification Using Sentinel-2 Imagery. *Sensors* **18**, 18 (2018).
20. Zhang, C., Li, G., Du, S., Tan, W. & Gao, F. Three-dimensional densely connected convolutional network for hyperspectral remote sensing image classification. *JARS* **13**, 016519 (2019).
21. Russakovsky, O. *et al.* ImageNet Large Scale Visual Recognition Challenge. Preprint at https://doi.org/10.48550/arXiv.1409.0575 (2015).
22. Kokol, P., Kokol, M. & Zagoranski, S. Machine learning on small size samples: A synthetic knowledge synthesis. *Science Progress* **105**, 00368504211029777 (2022).
23. Brigato, L. & Iocchi, L. A Close Look at Deep Learning with Small Data. Preprint at https://doi.org/10.48550/arXiv.2003.12843 (2020).
24. Lin, T.-Y. *et al.* Microsoft COCO: Common Objects in Context. Preprint at https://doi.org/10.48550/arXiv.1405.0312 (2015).
25. Kuznetsova, A. *et al.* The Open Images Dataset V4: Unified image classification, object detection, and visual relationship detection at scale. *Int J Comput Vis* **128**, 1956–1981 (2020).
26. Adadi, A. A survey on data-efficient algorithms in big data era. *Journal of Big Data* **8**, 24 (2021).

27. Du, S. S. *et al.* How Many Samples are Needed to Estimate a Convolutional or Recurrent Neural Network? Preprint at https://doi.org/10.48550/arXiv.1805.07883 (2019).
28. Tiny ImageNet. https://kaggle.com/competitions/tiny-imagenet.
29. Blekos, K., Nousias, S. & Lalos, A. S. Efficient automated U - Net based tree crown delineation using UAV multi-spectral imagery on embedded devices. in *2020 IEEE 18th International Conference on Industrial Informatics (INDIN)* vol. 1 541–546 (2020).
30. Freeman, D. *et al.* Watson on the Farm: Using Cloud-Based Artificial Intelligence to Identify Early Indicators of Water Stress. *Remote Sensing* **11**, 2645 (2019).
31. Hong-Yu, F. *et al.* Ramie Plant Counting Based on UAV Remote Sensing Technology and Deep Learning. *Journal of Natural Fibers* **20**, 2159610 (2023).
32. Li, L., Cao, G., Liu, J. & Tong, Y. Efficient Detection in Aerial Images for Resource-Limited Satellites. *IEEE Geoscience and Remote Sensing Letters* **19**, 1–5 (2022).
33. Liu, Y. & Zheng, F. Object-oriented and multi-scale target classification and recognition based on hierarchical ensemble learning. *Computers & Electrical Engineering* **62**, 538–554 (2017).
34. Malambo, L. *et al.* A Deep Learning Semantic Segmentation-Based Approach for Field-Level Sorghum Panicle Counting. *Remote Sensing* **11**, 2939 (2019).
35. Putra, Y. C. & Wijayanto, A. W. Automatic detection and counting of oil palm trees using remote sensing and object-based deep learning. *Remote Sensing Applications: Society and Environment* **29**, 100914 (2023).
36. Safonova, A. *et al.* Detection of Fir Trees (Abies sibirica) Damaged by the Bark Beetle in Unmanned Aerial Vehicle Images with Deep Learning. *Remote Sensing* **11**, 643 (2019).
37. Safonova, A., Guirado, E., Maglinets, Y., Alcaraz-Segura, D. & Tabik, S. Olive Tree Biovolume from UAV Multi-Resolution Image Segmentation with Mask R-CNN. *Sensors* **21**, 1617 (2021).
38. Safonova, A., Hamad, Y., Alekhina, A. & Kaplun, D. Detection of Norway Spruce Trees (Picea Abies) Infested by Bark Beetle in UAV Images Using YOLOs Architectures. *IEEE Access* **10**, 10384–10392 (2022).

39. Windrim, L., Bryson, M., McLean, M., Randle, J. & Stone, C. Automated Mapping of Woody Debris over Harvested Forest Plantations Using UAVs, High-Resolution Imagery, and Machine Learning. *Remote Sensing* **11**, 733 (2019).

40. Zenkl, R. *et al.* Outdoor Plant Segmentation With Deep Learning for High-Throughput Field Phenotyping on a Diverse Wheat Dataset. *Frontiers in Plant Science* **12**, (2022).

41. Dyrmann, M., Karstoft, H. & Midtiby, H. S. Plant species classification using deep convolutional neural network. *Biosystems Engineering* **151**, 72–80 (2016).

42. Guirado, E., Tabik, S., Alcaraz-Segura, D., Cabello, J. & Herrera, F. Deep-learning Versus OBIA for Scattered Shrub Detection with Google Earth Imagery: Ziziphus lotus as Case Study. *Remote Sensing* **9**, 1220 (2017).

43. Pang, Y. *et al.* Improved crop row detection with deep neural network for early-season maize stand count in UAV imagery. *Computers and Electronics in Agriculture* **178**, 105766 (2020).

44. Sapkota, B. B. *et al.* Use of synthetic images for training a deep learning model for weed detection and biomass estimation in cotton. *Sci Rep* **12**, 19580 (2022).

45. Liu, Z., Guan, R., Hu, J., Chen, W. & Li, X. Remote Sensing Scene Data Generation Using Element Geometric Transformation and GAN-Based Texture Synthesis. *Applied Sciences* **12**, 3972 (2022).

46. Nakkiran, P. *et al.* Deep Double Descent: Where Bigger Models and More Data Hurt. Preprint at https://doi.org/10.48550/arXiv.1912.02292 (2019).

47. Elhage, N. *et al.* Toy Models of Superposition. Preprint at https://doi.org/10.48550/arXiv.2209.10652 (2022).

48. Lecun, Y., Bottou, L., Bengio, Y. & Haffner, P. Gradient-based learning applied to document recognition. *Proceedings of the IEEE* **86**, 2278–2324 (1998).

49. Khan, A., Sohail, A., Zahoora, U. & Qureshi, A. S. A survey of the recent architectures of deep convolutional neural networks. *Artif Intell Rev* **53**, 5455–5516 (2020).

50. Dosovitskiy, A. *et al.* An Image is Worth 16x16 Words: Transformers for Image Recognition at Scale. Preprint at https://doi.org/10.48550/arXiv.2010.11929 (2021).

51. Dehghani, M. *et al.* Scaling Vision Transformers to 22 Billion Parameters. Preprint at https://doi.org/10.48550/arXiv.2302.05442 (2023).
52. Yuan, Q. *et al.* Deep learning in environmental remote sensing: Achievements and challenges. *Remote Sensing of Environment* **241**, 111716 (2020).
53. Osco, L. P. *et al.* A review on deep learning in UAV remote sensing. *International Journal of Applied Earth Observation and Geoinformation* **102**, 102456 (2021).
54. Lange, M., Feilhauer, H., Kühn, I. & Doktor, D. Mapping land-use intensity of grasslands in Germany with machine learning and Sentinel-2 time series. *Remote Sensing of Environment* **277**, 112888 (2022).
55. Li, M. & Stein, A. Mapping Land Use from High Resolution Satellite Images by Exploiting the Spatial Arrangement of Land Cover Objects. *Remote Sensing* **12**, 4158 (2020).
56. Odebiri, O., Mutanga, O. & Odindi, J. Deep learning-based national scale soil organic carbon mapping with Sentinel-3 data. *Geoderma* **411**, 115695 (2022).
57. Astolfi, G. *et al.* Combining Syntactic Methods With LSTM to Classify Soybean Aerial Images. *IEEE Geoscience and Remote Sensing Letters* **18**, 2182–2186 (2021).
58. Ho, B., Kocer, B. B. & Kovac, M. Vision based crown loss estimation for individual trees with remote aerial robots. *ISPRS Journal of Photogrammetry and Remote Sensing* **188**, 75–88 (2022).
59. Feng, F., Zhang, Y., Zhang, J. & Liu, B. Small Sample Hyperspectral Image Classification Based on Cascade Fusion of Mixed Spatial-Spectral Features and Second-Order Pooling. *Remote Sensing* **14**, 505 (2022).
60. Xue, Z. *et al.* Self-Supervised Feature Learning for Multimodal Remote Sensing Image Land Cover Classification. *IEEE Transactions on Geoscience and Remote Sensing* **60**, 1–15 (2022).
61. Sagan, V. *et al.* Field-scale crop yield prediction using multi-temporal WorldView-3 and PlanetScope satellite data and deep learning. *ISPRS Journal of Photogrammetry and Remote Sensing* **174**, 265–281 (2021).

62. Kim, W.-S. *et al.* Weakly Supervised Crop Area Segmentation for an Autonomous Combine Harvester. *Sensors* **21**, 4801 (2021).

63. Li, H. *et al.* Crop Classification Based on GDSSM-CNN Using Multi-Temporal RADARSAT-2 SAR with Limited Labeled Data. *Remote Sensing* **14**, 3889 (2022).

64. Zhao, H. *et al.* Evaluation of Three Deep Learning Models for Early Crop Classification Using Sentinel-1A Imagery Time Series—A Case Study in Zhanjiang, China. *Remote Sensing* **11**, 2673 (2019).

65. Muro, J. *et al.* Predicting plant biomass and species richness in temperate grasslands across regions, time, and land management with remote sensing and deep learning. *Remote Sensing of Environment* **282**, 113262 (2022).

66. Lioutas, V. Mapping Low-Resolution Images To Multiple High-Resolution Images Using Non-Adversarial Mapping. Preprint at https://doi.org/10.48550/arXiv.2006.11708 (2020).

67. Sanlang, S. *et al.* Integrating Aerial LiDAR and Very-High-Resolution Images for Urban Functional Zone Mapping. *Remote Sensing* **13**, 2573 (2021).

68. Uhl, J. H. *et al.* Combining Remote-Sensing-Derived Data and Historical Maps for Long-Term Back-Casting of Urban Extents. *Remote Sensing* **13**, 3672 (2021).

69. Chen, Y., Zhao, X. & Jia, X. Spectral–Spatial Classification of Hyperspectral Data Based on Deep Belief Network. *IEEE Journal of Selected Topics in Applied Earth Observations and Remote Sensing* **8**, 2381–2392 (2015).

70. Pan, B., Shi, Z., Zhang, N. & Xie, S. Hyperspectral Image Classification Based on Nonlinear Spectral–Spatial Network. *IEEE Geoscience and Remote Sensing Letters* **13**, 1782–1786 (2016).

71. Jia, S. *et al.* A survey: Deep learning for hyperspectral image classification with few labeled samples. *Neurocomputing* **448**, 179–204 (2021).

72. Pan, B., Shi, Z. & Xu, X. MugNet: Deep learning for hyperspectral image classification using limited samples. *ISPRS Journal of Photogrammetry and Remote Sensing* **145**, 108–119 (2018).

73. Ding, C. *et al.* Integrating Hybrid Pyramid Feature Fusion and Coordinate Attention for Effective Small Sample Hyperspectral Image Classification. *Remote Sensing* **14**, 2355 (2022).

74. Gao, H. *et al.* Pixel-Level Prediction for Ocean Remote Sensing Image Features Fusion Based on Global and Local Semantic Relations. *IEEE Access* **9**, 11644–11654 (2021).

75. Wang, Z., Zou, C. & Cai, W. Small Sample Classification of Hyperspectral Remote Sensing Images Based on Sequential Joint Deeping Learning Model. *IEEE Access* **8**, 71353–71363 (2020).

76. Wu, C. *et al.* Convolutional Neural Network with Expert Knowledge for Hyperspectral Remote Sensing Imagery Classification. *KSII Transactions on Internet and Information Systems* **13**, 3917–3941 (2019).

77. Xu, Y. *et al.* Residual Spatial Attention Kernel Generation Network for Hyperspectral Image Classification With Small Sample Size. *IEEE Transactions on Geoscience and Remote Sensing* **60**, 1–14 (2022).

78. Zuo, X. *et al.* Graph inductive learning method for small sample classification of hyperspectral remote sensing images. *European Journal of Remote Sensing* **53**, 349–357 (2020).

79. Gao, K. *et al.* Small sample classification of hyperspectral image using model-agnostic meta-learning algorithm and convolutional neural network. *International Journal of Remote Sensing* **42**, 3090–3122 (2021).

80. Kang, X., Zhuo, B. & Duan, P. Semi-supervised deep learning for hyperspectral image classification. *Remote Sensing Letters* **10**, 353–362 (2019).

81. Kato, S. *et al.* Automated classification of heat sources detected using SWIR remote sensing. *International Journal of Applied Earth Observation and Geoinformation* **103**, 102491 (2021).

82. Xue, Z., Lin, H. & Wang, F. A Small Target Forest Fire Detection Model Based on YOLOv5 Improvement. *Forests* **13**, 1332 (2022).

83. Shin, J., Khim, B.-K., Jang, L.-H., Lim, J. & Jo, Y.-H. Convolutional neural network model for discrimination of harmful algal bloom (HAB) from non-HABs using Sentinel-3 OLCI imagery. *ISPRS Journal of Photogrammetry and Remote Sensing* **191**, 250–262 (2022).

84. Leitão, P. J. *et al.* From sample to pixel: multi-scale remote sensing data for upscaling aboveground carbon data in heterogeneous landscapes. *Ecosphere* **9**, e02298 (2018).

85. Kattenborn, T., Lopatin, J., Förster, M., Braun, A. C. & Fassnacht, F. E. UAV data as alternative to field sampling to map woody invasive species based on combined Sentinel-1 and Sentinel-2 data. *Remote Sensing of Environment* **227**, 61–73 (2019).

86. Shorten, C. & Khoshgoftaar, T. M. A survey on Image Data Augmentation for Deep Learning. *Journal of Big Data* **6**, 60 (2019).

87. Reedha, R., Dericquebourg, E., Canals, R. & Hafiane, A. Transformer Neural Network for Weed and Crop Classification of High Resolution UAV Images. *Remote Sensing* **14**, 592 (2022).

88. Yu, M., Rui, X., Xie, W., Xu, X. & Wei, W. Research on Automatic Identification Method of Terraces on the Loess Plateau Based on Deep Transfer Learning. *Remote Sensing* **14**, 2446 (2022).

89. Wang, D. *et al.* SSRNet: In-Field Counting Wheat Ears Using Multi-Stage Convolutional Neural Network. *IEEE Transactions on Geoscience and Remote Sensing* **60**, 1–11 (2022).

90. Barbosa, B. D. S. *et al.* UAV-based coffee yield prediction utilizing feature selection and deep learning. *Smart Agricultural Technology* **1**, 100010 (2021).

91. Khan, A. H., Fraz, M. M. & Shahzad, M. Deep Learning Based Land Cover and Crop Type Classification: A Comparative Study. in *2021 International Conference on Digital Futures and Transformative Technologies (ICoDT2)* 1–6 (2021). doi:10.1109/ICoDT252288.2021.9441483.

92. Althnian, A. *et al.* Impact of Dataset Size on Classification Performance: An Empirical Evaluation in the Medical Domain. *Applied Sciences* **11**, 796 (2021).

93. Prusa, J., Khoshgoftaar, T. M. & Seliya, N. The Effect of Dataset Size on Training Tweet Sentiment Classifiers. in *2015 IEEE 14th International Conference on Machine Learning and Applications (ICMLA)* 96–102 (2015). doi:10.1109/ICMLA.2015.22.

94. Katsaragakis, M., Papadopoulos, L., Konijnenburg, M., Catthoor, F. & Soudris, D. Memory Footprint Optimization Techniques for Machine Learning Applications in Embedded Systems. in

2020 IEEE International Symposium on Circuits and Systems (ISCAS) 1–4 (2020). doi:10.1109/ISCAS45731.2020.9181038.

95. D'souza, R. N., Huang, P.-Y. & Yeh, F.-C. Structural Analysis and Optimization of Convolutional Neural Networks with a Small Sample Size. *Sci Rep* **10**, 834 (2020).
96. Elsken, T., Metzen, J.-H. & Hutter, F. Simple And Efficient Architecture Search for Convolutional Neural Networks. Preprint at https://doi.org/10.48550/arXiv.1711.04528 (2017).
97. Keshari, R., Vatsa, M., Singh, R. & Noore, A. Learning Structure and Strength of CNN Filters for Small Sample Size Training. Preprint at https://doi.org/10.48550/arXiv.1803.11405 (2018).
98. Liu, S. & Deng, W. Very deep convolutional neural network based image classification using small training sample size. in *2015 3rd IAPR Asian Conference on Pattern Recognition (ACPR)* 730–734 (2015). doi:10.1109/ACPR.2015.7486599.
99. Wang, H., Duentsch, I., Guo, G. & Khan, S. A. Special issue on small data analytics. *Int. J. Mach. Learn. & Cyber.* **14**, 1–2 (2023).
100. Zhao, W. Research on the deep learning of the small sample data based on transfer learning. *AIP Conference Proceedings* **1864**, 020018 (2017).
101. Liu, B., Wei, Y., Zhang, Y. & Yang, Q. Deep Neural Networks for High Dimension, Low Sample Size Data. 2287–2293 (2017) doi:https://doi.org/10.24963/ijcai.2017/318.
102. Bailly, A. *et al.* Effects of dataset size and interactions on the prediction performance of logistic regression and deep learning models. *Computer Methods and Programs in Biomedicine* **213**, 106504 (2022).
103. Power, A., Burda, Y., Edwards, H., Babuschkin, I. & Misra, V. Grokking: Generalization Beyond Overfitting on Small Algorithmic Datasets. Preprint at https://doi.org/10.48550/arXiv.2201.02177 (2022).
104. Wu, X., Chen, C., Zhong, M., Wang, J. & Shi, J. COVID-AL: The diagnosis of COVID-19 with deep active learning. *Medical Image Analysis* **68**, 101913 (2021).

105. Schat, E., Schoot, R. van de, Kouw, W. M., Veen, D. & Mendrik, A. M. The data representativeness criterion: Predicting the performance of supervised classification based on data set similarity. *PLOS ONE* **15**, e0237009 (2020).

106. Lones, M. A. How to avoid machine learning pitfalls: a guide for academic researchers. Preprint at https://doi.org/10.48550/arXiv.2108.02497 (2023).

107. Iman, M., Rasheed, K. & Arabnia, H. R. A Review of Deep Transfer Learning and Recent Advancements. Preprint at https://doi.org/10.48550/arXiv.2201.09679 (2022).

108. Rawat, W. & Wang, Z. Deep Convolutional Neural Networks for Image Classification: A Comprehensive Review. *Neural Computation* **29**, 2352–2449 (2017).

109. Dong, X., Tuan, L. A., Lin, M., Yan, S. & Zhang, H. How Should Pre-Trained Language Models Be Fine-Tuned Towards Adversarial Robustness? Preprint at https://doi.org/10.48550/arXiv.2112.11668 (2021).

110. Ziegler, D. M. *et al.* Fine-Tuning Language Models from Human Preferences. Preprint at https://doi.org/10.48550/arXiv.1909.08593 (2020).

111. Wang, S. *et al.* A deep learning framework for remote sensing image registration. *ISPRS Journal of Photogrammetry and Remote Sensing* **145**, 148–164 (2018).

112. Zhang, H. *et al.* Hyperspectral Classification Based on Lightweight 3-D-CNN With Transfer Learning. *IEEE Transactions on Geoscience and Remote Sensing* **57**, 5813–5828 (2019).

113. Hou, Y. *et al.* Radar-Jamming Classification in the Event of Insufficient Samples Using Transfer Learning. *Symmetry* **14**, 2318 (2022).

114. Lv, Q. *et al.* Radar Deception Jamming Recognition Based on Weighted Ensemble CNN With Transfer Learning. *IEEE Transactions on Geoscience and Remote Sensing* **60**, 1–11 (2022).

115. Character, L., Ortiz JR, A., Beach, T. & Luzzadder-Beach, S. Archaeologic Machine Learning for Shipwreck Detection Using Lidar and Sonar. *Remote Sensing* **13**, 1759 (2021).

116. Wang, S. *et al.* Weed Density Extraction Based on Few-Shot Learning Through UAV Remote Sensing RGB and Multispectral Images in Ecological Irrigation Area. *Frontiers in Plant Science* **12**, (2022).

117. Zhao, W., Yamada, W., Li, T., Digman, M. & Runge, T. Augmenting Crop Detection for Precision Agriculture with Deep Visual Transfer Learning—A Case Study of Bale Detection. *Remote Sensing* **13**, 23 (2021).

118. Chen, J., Sun, J., Li, Y. & Hou, C. Object detection in remote sensing images based on deep transfer learning. *Multimed Tools Appl* **81**, 12093–12109 (2022).

119. Yang, W., Zhang, X. & Luo, P. Transferability of Convolutional Neural Network Models for Identifying Damaged Buildings Due to Earthquake. *Remote Sensing* **13**, 504 (2021).

120. Naushad, R., Kaur, T. & Ghaderpour, E. Deep Transfer Learning for Land Use and Land Cover Classification: A Comparative Study. *Sensors* **21**, 8083 (2021).

121. Qiu, T. *et al.* Using different training strategies for urban land-use classification based on convolutional neural networks. *Frontiers in Environmental Science* **10**, (2022).

122. El Zini, J., Rizk, Y. & Awad, M. A Deep Transfer Learning Framework for Seismic Data Analysis: A Case Study on Bright Spot Detection. *IEEE Transactions on Geoscience and Remote Sensing* **58**, 3202–3212 (2020).

123. Abu, M. *et al.* A Comprehensive Performance Analysis of Transfer Learning Optimization in Visual Field Defect Classification. *Diagnostics* **12**, 1258 (2022).

124. Sharma, P., Amhia, H. & Sharma, S. D. Performance analysis of pre-trained transfer learning models for the classification of the rolling bearing faults. *J. Phys.: Conf. Ser.* **2070**, 012141 (2021).

125. Rani, V., Nabi, S. T., Kumar, M., Mittal, A. & Kumar, K. Self-supervised Learning: A Succinct Review. *Arch Computat Methods Eng* (2023) doi:10.1007/s11831-023-09884-2.

126. Chen, L. *et al.* Self-supervised learning for medical image analysis using image context restoration. *Medical Image Analysis* **58**, 101539 (2019).

127. Krishnan, R., Rajpurkar, P. & Topol, E. J. Self-supervised learning in medicine and healthcare. *Nat. Biomed. Eng* **6**, 1346–1352 (2022).

128. Ma, W. & Liu, Y. A data-efficient self-supervised deep learning model for design and characterization of nanophotonic structures. *Sci. China Phys. Mech. Astron.* **63**, 284212 (2020).

129. Mohamed, A. *et al.* Self-Supervised Speech Representation Learning: A Review. *IEEE J. Sel. Top. Signal Process.* **16**, 1179–1210 (2022).

130. Pöppelbaum, J., Chadha, G. S. & Schwung, A. Contrastive learning based self-supervised time-series analysis. *Applied Soft Computing* **117**, 108397 (2022).

131. Jing, L. & Tian, Y. Self-supervised Visual Feature Learning with Deep Neural Networks: A Survey. Preprint at https://doi.org/10.48550/arXiv.1902.06162 (2019).

132. Wang, Z., Hou, C., Yue, G. & Yang, Q. Dynamic-boosting attention for self-supervised video representation learning. *Appl Intell* **52**, 3143–3155 (2022).

133. Yan, X. *et al.* Self-Supervised Learning to Detect Key Frames in Videos. *Sensors (Basel)* **20**, 6941 (2020).

134. Hsu, W.-N. *et al.* HuBERT: Self-Supervised Speech Representation Learning by Masked Prediction of Hidden Units. Preprint at https://doi.org/10.48550/arXiv.2106.07447 (2021).

135. Yuan, D., Chang, X., Huang, P.-Y., Liu, Q. & He, Z. Self-Supervised Deep Correlation Tracking. *IEEE Transactions on Image Processing* **30**, 976–985 (2021).

136. Liu, X. *et al.* Dense Depth Estimation in Monocular Endoscopy with Self-supervised Learning Methods. Preprint at https://doi.org/10.48550/arXiv.1902.07766 (2019).

137. Li, X., Jia, M., Islam, M. T., Yu, L. & Xing, L. Self-supervised Feature Learning via Exploiting Multi-modal Data for Retinal Disease Diagnosis. Preprint at https://doi.org/10.48550/arXiv.2007.11067 (2020).

138. Liu, F., Kijowski, R., El Fakhri, G. & Feng, L. Magnetic resonance parameter mapping using model-guided self-supervised deep learning. *Magnetic Resonance in Medicine* **85**, 3211–3226 (2021).

139. Yaman, B. *et al.* Self-supervised learning of physics-guided reconstruction neural networks without fully sampled reference data. *Magnetic Resonance in Medicine* **84**, 3172–3191 (2020).

140. Zhu, J. *et al.* Rubik's Cube+: A self-supervised feature learning framework for 3D medical image analysis. *Medical Image Analysis* **64**, 101746 (2020).

141. Wang, C., Wang, X., Bai, X., Liu, Y. & Zhou, J. Self-Supervised deep homography estimation with invertibility constraints. *Pattern Recognition Letters* **128**, 355–360 (2019).

142. Liu, B. *et al.* ES2FL: Ensemble Self-Supervised Feature Learning for Small Sample Classification of Hyperspectral Images. *Remote Sensing* **14**, 4236 (2022).

143. Rangnekar, A., Mokashi, N., Ientilucci, E. J., Kanan, C. & Hoffman, M. J. AeroRIT: A New Scene for Hyperspectral Image Analysis. *IEEE Trans. Geosci. Remote Sensing* **58**, 8116–8124 (2020).

144. Song, L., Feng, Z., Yang, S., Zhang, X. & Jiao, L. Self-Supervised Assisted Semi-Supervised Residual Network for Hyperspectral Image Classification. *Remote Sensing* **14**, 2997 (2022).

145. Cao, Y.-H. & Wu, J. Rethinking Self-Supervised Learning: Small is Beautiful. Preprint at https://doi.org/10.48550/arXiv.2103.13559 (2021).

146. Su, J.-C., Maji, S. & Hariharan, B. When Does Self-supervision Improve Few-shot Learning? Preprint at https://doi.org/10.48550/arXiv.1910.03560 (2020).

147. Han, M., Wu, H., Chen, Z., Li, M. & Zhang, X. A survey of multi-label classification based on supervised and semi-supervised learning. *Int. J. Mach. Learn. & Cyber.* (2022) doi:10.1007/s13042-022-01658-9.

148. Wang, L. *et al.* Semi-Supervised Dual Relation Learning for Multi-Label Classification. *IEEE Transactions on Image Processing* **30**, 9125–9135 (2021).

149. Ma, W., Cheng, F., Xu, Y., Wen, Q. & Liu, Y. Probabilistic representation and inverse design of metamaterials based on a deep generative model with semi-supervised learning strategy. Preprint at https://doi.org/10.48550/arXiv.1901.10819 (2019).

150. BalaAnand, M. *et al.* An enhanced graph-based semi-supervised learning algorithm to detect fake users on Twitter. *J Supercomput* **75**, 6085–6105 (2019).

151. Xu, Z., Wang, H. & Yang, Y. Semi-supervised self-growing generative adversarial networks for image recognition. *Multimed Tools Appl* **80**, 17461–17486 (2021).

152. Rostami, M., Berahmand, K. & Forouzandeh, S. A novel method of constrained feature selection by the measurement of pairwise constraints uncertainty. *Journal of Big Data* **7**, 83 (2020).

153. Tseng, K.-K., Zhang, R., Chen, C.-M. & Hassan, M. M. DNetUnet: a semi-supervised CNN of medical image segmentation for super-computing AI service. *J Supercomput* **77**, 3594–3615 (2021).

154. Shim, S., Kim, J., Lee, S.-W. & Cho, G.-C. Road damage detection using super-resolution and semi-supervised learning with generative adversarial network. *Automation in Construction* **135**, 104139 (2022).

155. Lu, S. *et al.* An Improved Algorithm of Drift Compensation for Olfactory Sensors. *Applied Sciences* **12**, 9529 (2022).

156. Feng, Y. *et al.* Semi-supervised meta-learning networks with squeeze-and-excitation attention for few-shot fault diagnosis. *ISA Transactions* **120**, 383–401 (2022).

157. Jozdani, S. *et al.* Leveraging Deep Neural Networks to Map Caribou Lichen in High-Resolution Satellite Images Based on a Small-Scale, Noisy UAV-Derived Map. *Remote Sensing* **13**, 2658 (2021).

158. Chapelle, O., Scholkopf, B. & Zien, A., Eds. Semi-Supervised Learning (Chapelle, O. et al., Eds.; 2006) [Book reviews]. *IEEE Transactions on Neural Networks* **20**, 542–542 (2009).

159. He, J. *et al.* Rethinking Re-Sampling in Imbalanced Semi-Supervised Learning. Preprint at https://doi.org/10.48550/arXiv.2106.00209 (2021).

160. Hospedales, T., Antoniou, A., Micaelli, P. & Storkey, A. Meta-Learning in Neural Networks: A Survey. Preprint at https://doi.org/10.48550/arXiv.2004.05439 (2020).

161. Li, Y. & Yang, J. Meta-learning baselines and database for few-shot classification in agriculture. *Computers and Electronics in Agriculture* **182**, 106055 (2021).

162. Zhang, P., Bai, Y., Wang, D., Bai, B. & Li, Y. Few-Shot Classification of Aerial Scene Images via Meta-Learning. *Remote Sensing* **13**, 108 (2021).

163. Zuo, X., Yu, X., Liu, B., Zhang, P. & Tan, X. FSL-EGNN: Edge-Labeling Graph Neural Network for Hyperspectral Image Few-Shot Classification. *IEEE Transactions on Geoscience and Remote Sensing* **60**, 1–18 (2022).

164. Li, Z. *et al.* Deep Cross-Domain Few-Shot Learning for Hyperspectral Image Classification. *IEEE Transactions on Geoscience and Remote Sensing* **60**, 1–18 (2022).

165. Goodfellow, I. J. *et al.* Generative Adversarial Networks. Preprint at https://doi.org/10.48550/arXiv.1406.2661 (2014).

166. Yi, X., Walia, E. & Babyn, P. Generative Adversarial Network in Medical Imaging: A Review. *Medical Image Analysis* **58**, 101552 (2019).

167. Liu, X., Wang, Y. & Liu, Q. Psgan: A Generative Adversarial Network for Remote Sensing Image Pan-Sharpening. in *2018 25th IEEE International Conference on Image Processing (ICIP)* 873–877 (2018). doi:10.1109/ICIP.2018.8451049.

168. Zhong, Z., Li, J., Clausi, D. A. & Wong, A. Generative Adversarial Networks and Conditional Random Fields for Hyperspectral Image Classification. *IEEE Trans. Cybern.* **50**, 3318–3329 (2020).

169. Zhu, L., Chen, Y., Ghamisi, P. & Benediktsson, J. A. Generative Adversarial Networks for Hyperspectral Image Classification. *IEEE Transactions on Geoscience and Remote Sensing* **56**, 5046–5063 (2018).

170. Bai, J. *et al.* Few-Shot Hyperspectral Image Classification Based on Adaptive Subspaces and Feature Transformation. *IEEE Transactions on Geoscience and Remote Sensing* **60**, 1–17 (2022).

171. Liu, J. *et al.* An Investigation of a Multidimensional CNN Combined with an Attention Mechanism Model to Resolve Small-Sample Problems in Hyperspectral Image Classification. *Remote Sensing* **14**, 785 (2022).

172. Rao, M., Tang, P. & Zhang, Z. Spatial–Spectral Relation Network for Hyperspectral Image Classification With Limited Training Samples. *IEEE Journal of Selected Topics in Applied Earth Observations and Remote Sensing* **12**, 5086–5100 (2019).

173. Wang, T., Liu, H. & Li, J. Spectral–Spatial Classification of Few Shot Hyperspectral Image With Deep 3-D Convolutional Random Fourier Features Network. *IEEE Transactions on Geoscience and Remote Sensing* **60**, 1–18 (2022).

174. Liu, B. *et al.* Deep Few-Shot Learning for Hyperspectral Image Classification. *IEEE Transactions on Geoscience and Remote Sensing* **57**, 2290–2304 (2019).

175. Wang, Y., Yao, Q., Kwok, J. & Ni, L. M. Generalizing from a Few Examples: A Survey on Few-Shot Learning. Preprint at https://doi.org/10.48550/arXiv.1904.05046 (2020).

176. Wang, G. *et al.* Interactive Medical Image Segmentation using Deep Learning with Image-specific Fine-tuning. *IEEE Trans. Med. Imaging* **37**, 1562–1573 (2018).

177. Lampert, C. H., Nickisch, H. & Harmeling, S. Attribute-Based Classification for Zero-Shot Visual Object Categorization. *IEEE Transactions on Pattern Analysis and Machine Intelligence* **36**, 453–465 (2014).

178. Akata, Z., Perronnin, F., Harchaoui, Z. & Schmid, C. Label-Embedding for Image Classification. *IEEE Trans. Pattern Anal. Mach. Intell.* **38**, 1425–1438 (2016).

179. Sumbul, G., Charfuelan, M., Demir, B. & Markl, V. BigEarthNet: A Large-Scale Benchmark Archive For Remote Sensing Image Understanding. in *IGARSS 2019 - 2019 IEEE International Geoscience and Remote Sensing Symposium* 5901–5904 (2019). doi:10.1109/IGARSS.2019.8900532.

180. Villon, S. *et al.* Automatic underwater fish species classification with limited data using few-shot learning. *Ecological Informatics* **63**, 101320 (2021).

181. Ren, P. *et al.* A Survey of Deep Active Learning. Preprint at https://doi.org/10.48550/arXiv.2009.00236 (2021).

182. Settles, B. *Active Learning Literature Survey*. https://minds.wisconsin.edu/handle/1793/60660 (2009).

183. Arora, S. & Agarwal, S. *Active Learning for Natural Language Processing. Literature Review*. vol. 2 (Language Technology Institute, Scool of Computer Scince, Carnegie Mellon University, 2007).

184. Zhang, C. *et al.* Multi-Species Individual Tree Segmentation and Identification Based on Improved Mask R-CNN and UAV Imagery in Mixed Forests. *Remote Sensing* **14**, 874 (2022).

185. Takezoe, R. *et al.* Deep Active Learning for Computer Vision: Past and Future. Preprint at https://doi.org/10.1561/116.00000057 (2022).

186. Wu, M., Li, C. & Yao, Z. Deep Active Learning for Computer Vision Tasks: Methodologies, Applications, and Challenges. *Applied Sciences* **12**, 8103 (2022).

187. Liu, P., Zhang, H. & Eom, K. B. Active Deep Learning for Classification of Hyperspectral Images. *IEEE Journal of Selected Topics in Applied Earth Observations and Remote Sensing* **10**, 712–724 (2017).

188. Cao, X., Yao, J., Xu, Z. & Meng, D. Hyperspectral Image Classification With Convolutional Neural Network and Active Learning. *IEEE Transactions on Geoscience and Remote Sensing* **58**, 4604–4616 (2020).

189. Zhou, Z.-H. A brief introduction to weakly supervised learning. *National Science Review* **5**, 44–53 (2018).

190. Liu, Y., Chen, P., Zhang, J., Liu, N. & Liu, Y. Weakly Supervised Ternary Stream Data Augmentation Fine-Grained Classification Network for Identifying Acute Lymphoblastic Leukemia. *Diagnostics* **12**, 16 (2022).

191. Wu, X. *et al.* IDA-MIL: Classification of Glomerular with Spike-like Projections via Multiple Instance Learning with Instance-level Data Augmentation. *Computer Methods and Programs in Biomedicine* **225**, 107106 (2022).

192. Ruan, H., Wang, Y., Li, X., Qin, Y. & Tang, B. An enhanced non-local weakly supervised fault diagnosis method for rotating machinery. *Measurement* **189**, 110433 (2022).

193. Cheng, G. & Han, J. A survey on object detection in optical remote sensing images. *ISPRS Journal of Photogrammetry and Remote Sensing* **117**, 11–28 (2016).

194. Han, J., Zhang, D., Cheng, G., Guo, L. & Ren, J. Object Detection in Optical Remote Sensing Images Based on Weakly Supervised Learning and High-Level Feature Learning. *IEEE Transactions on Geoscience and Remote Sensing* **53**, 3325–3337 (2015).

195. Wei, Y. & Ji, S. Scribble-based Weakly Supervised Deep Learning for Road Surface Extraction from Remote Sensing Images. Preprint at https://doi.org/10.48550/arXiv.2010.13106 (2020).

196. Yao, X., Han, J., Cheng, G., Qian, X. & Guo, L. Semantic Annotation of High-Resolution Satellite Images via Weakly Supervised Learning. *IEEE Transactions on Geoscience and Remote Sensing* **54**, 3660–3671 (2016).

197. Zhang, Y. & Yang, Q. An overview of multi-task learning. *National Science Review* **5**, 30–43 (2018).

198. Ruder, S. An Overview of Multi-Task Learning in Deep Neural Networks. Preprint at https://doi.org/10.48550/arXiv.1706.05098 (2017).

199. Sosnin, S. *et al.* A Survey of Multi-task Learning Methods in Chemoinformatics. *Molecular Informatics* **38**, 1800108 (2019).

200. Zhao, Y., Wang, X., Che, T., Bao, G. & Li, S. Multi-task deep learning for medical image computing and analysis: A review. *Computers in Biology and Medicine* **153**, 106496 (2023).

201. Qi, K., Liu, W., Yang, C., Guan, Q. & Wu, H. Multi-Task Joint Sparse and Low-Rank Representation for the Scene Classification of High-Resolution Remote Sensing Image. *Remote Sensing* **9**, 10 (2017).

202. Wu, X., Zhang, X., Wang, N. & Cen, Y. Joint Sparse and Low-Rank Multi-Task Learning with Extended Multi-Attribute Profile for Hyperspectral Target Detection. *Remote Sensing* **11**, 150 (2019).

203. Zhang, Y., Wu, K., Du, B., Zhang, L. & Hu, X. Hyperspectral Target Detection via Adaptive Joint Sparse Representation and Multi-Task Learning with Locality Information. *Remote Sensing* **9**, 482 (2017).

204. Li, Y. *et al.* MQANet: Multi-Task Quadruple Attention Network of Multi-Object Semantic Segmentation from Remote Sensing Images. *Remote Sensing* **14**, 6256 (2022).

205. Volpi, M. & Tuia, D. Deep multi-task learning for a geographically-regularized semantic segmentation of aerial images. *ISPRS Journal of Photogrammetry and Remote Sensing* **144**, 48–60 (2018).

206. Xiong, W., Lv, Y., Cui, Y., Zhang, X. & Gu, X. A Discriminative Feature Learning Approach for Remote Sensing Image Retrieval. *Remote Sensing* **11**, 281 (2019).

207. Zhao, P., Huang, L., Xin, Y., Guo, J. & Pan, Z. Multi-Aspect SAR Target Recognition Based on Prototypical Network with a Small Number of Training Samples. *Sensors* **21**, 4333 (2021).

208. Zhang, Y. & Xin, D. A Diverse Ensemble Deep Learning Method for Short-Term Traffic Flow Prediction Based on Spatiotemporal Correlations. *IEEE Transactions on Intelligent Transportation Systems* **23**, 16715–16727 (2022).

209. Hamdy, W., Ismail, A., Awad, W. A., Ibrahim, A. H. & Hassanien, A. E. An Optimized Ensemble Deep Learning Model for Predicting Plant miRNA–IncRNA Based on Artificial Gorilla Troops Algorithm. *Sensors* **23**, 2219 (2023).

210. Hu, H. *et al.* Driver identification through vehicular CAN bus data: An ensemble deep learning approach. *IET Intelligent Transport Systems* **n/a**,.

211. Ganaie, M. A., Hu, M., Malik, A. K., Tanveer, M. & Suganthan, P. N. Ensemble deep learning: A review. *Engineering Applications of Artificial Intelligence* **115**, 105151 (2022).

212. Karniadakis, G. E. *et al.* Physics-informed machine learning. *Nat Rev Phys* **3**, 422–440 (2021).

213. Vabalas, A., Gowen, E., Poliakoff, E. & Casson, A. J. Machine learning algorithm validation with a limited sample size. *PLOS ONE* **14**, e0224365 (2019).

214. Ying, X. An Overview of Overfitting and its Solutions. *J. Phys.: Conf. Ser.* **1168**, 022022 (2019).

215. Little, M. A. *et al.* Using and understanding cross-validation strategies. Perspectives on Saeb et al. *GigaScience* **6**, gix020 (2017).

216. Kattenborn, T. *et al.* Spatially autocorrelated training and validation samples inflate performance assessment of convolutional neural networks. *ISPRS Open Journal of Photogrammetry and Remote Sensing* **5**, 100018 (2022).

217. Le Rest, K., Pinaud, D., Monestiez, P., Chadoeuf, J. & Bretagnolle, V. Spatial leave-one-out cross-validation for variable selection in the presence of spatial autocorrelation. *Global Ecology and Biogeography* **23**, 811–820 (2014).

218. Ploton, P. *et al.* Spatial validation reveals poor predictive performance of large-scale ecological mapping models. *Nat Commun* **11**, 4540 (2020).

219. Roberts, D. R. *et al.* Cross-validation strategies for data with temporal, spatial, hierarchical, or phylogenetic structure. *Ecography* **40**, 913–929 (2017).

220. Xue, T. *et al.* Spatiotemporal continuous estimates of PM2.5 concentrations in China, 2000-2016: A machine learning method with inputs from satellites, chemical transport model, and ground observations. *Environ Int* **123**, 345–357 (2019).

221. Chen, G. *et al.* A machine learning method to estimate PM2.5 concentrations across China with remote sensing, meteorological and land use information. *Science of The Total Environment* **636**, 52–60 (2018).

222. Yang, S. *et al.* Modeling grassland above-ground biomass based on artificial neural network and remote sensing in the Three-River Headwaters Region. *Remote Sensing of Environment* **204**, 448–455 (2018).

223. Forkuor, G., Hounkpatin, O. K. L., Welp, G. & Thiel, M. High Resolution Mapping of Soil Properties Using Remote Sensing Variables in South-Western Burkina Faso: A Comparison of Machine Learning and Multiple Linear Regression Models. *PLOS ONE* **12**, e0170478 (2017).

224. Gibson, R., Danaher, T., Hehir, W. & Collins, L. A remote sensing approach to mapping fire severity in south-eastern Australia using sentinel 2 and random forest. *Remote Sensing of Environment* **240**, 111702 (2020).

225. Rigge, M. *et al.* Quantifying Western U.S. Rangelands as Fractional Components with Multi-Resolution Remote Sensing and In Situ Data. *Remote Sensing* **12**, 412 (2020).

226. Wu, Z., Liu, J., Yang, J., Xiao, Z. & Xiao, L. Composite kernel learning network for hyperspectral image classification. *International Journal of Remote Sensing* **42**, 6066–6089 (2021).

227. Keshari, R., Ghosh, S., Chhabra, S., Vatsa, M. & Singh, R. Unravelling Small Sample Size Problems in the Deep Learning World. Preprint at https://doi.org/10.48550/arXiv.2008.03522 (2020).

228. dos Santos Ferreira, A., Matte Freitas, D., Gonçalves da Silva, G., Pistori, H. & Theophilo Folhes, M. Weed detection in soybean crops using ConvNets. *Computers and Electronics in Agriculture* **143**, 314–324 (2017).

229. Di Cicco, M., Potena, C., Grisetti, G. & Pretto, A. Automatic model based dataset generation for fast and accurate crop and weeds detection. in *2017 IEEE/RSJ International Conference on Intelligent Robots and Systems (IROS)* 5188–5195 (2017). doi:10.1109/IROS.2017.8206408.

230. Fuentes, A., Yoon, S., Kim, S. C. & Park, D. S. A Robust Deep-Learning-Based Detector for Real-Time Tomato Plant Diseases and Pests Recognition. *Sensors* **17**, 2022 (2017).

231. Zhou, X. *et al.* A method for extracting the leaf litter distribution area in forest using chip feature. *International Journal of Remote Sensing* **39**, 5310–5329 (2018).

232. Chew, R. F. *et al.* Residential scene classification for gridded population sampling in developing countries using deep convolutional neural networks on satellite imagery. *International Journal of Health Geographics* **17**, 12 (2018).

233. Barbedo, J. G. A., Koenigkan, L. V., Santos, T. T. & Santos, P. M. A Study on the Detection of Cattle in UAV Images Using Deep Learning. *Sensors* **19**, 5436 (2019).

234. Xue, W., Dai, X. & Liu, L. Remote Sensing Scene Classification Based on Multi-Structure Deep Features Fusion. *IEEE Access* **8**, 28746–28755 (2020).

235. Zhang, F., Wang, Y., Ni, J., Zhou, Y. & Hu, W. SAR Target Small Sample Recognition Based on CNN Cascaded Features and AdaBoost Rotation Forest. *IEEE Geoscience and Remote Sensing Letters* **17**, 1008–1012 (2020).

236. Li, B. *et al.* Further Exploring Convolutional Neural Networks' Potential for Land-Use Scene Classification. *IEEE Geoscience and Remote Sensing Letters* **17**, 1687–1691 (2020).

237. Zhou, X., Tang, T., Cui, Y., Zhang, L. & Kuang, G. Novel Loss Function in CNN for Small Sample Target Recognition in SAR Images. *IEEE Geoscience and Remote Sensing Letters* **19**, 1–5 (2022).

238. Han, Y. *et al.* Combining 3D-CNN and Squeeze-and-Excitation Networks for Remote Sensing Sea Ice Image Classification. *Mathematical Problems in Engineering* **2020**, e8065396 (2020).

239. Chew, R. *et al.* Deep Neural Networks and Transfer Learning for Food Crop Identification in UAV Images. *Drones* **4**, 7 (2020).

240. Liu, C. *et al.* Urban Land Cover Classification of High-Resolution Aerial Imagery Using a Relation-Enhanced Multiscale Convolutional Network. *Remote Sensing* **12**, 311 (2020).

241. Tian, X., Chen, L., Zhang, X. & Chen, E. Improved Prototypical Network Model for Forest Species Classification in Complex Stand. *Remote Sensing* **12**, 3839 (2020).

242. He, M.-X., Hao, P. & Xin, Y.-Z. A Robust Method for Wheatear Detection Using UAV in Natural Scenes. *IEEE Access* **8**, 189043–189053 (2020).

243. Su, D., Kong, H., Qiao, Y. & Sukkarieh, S. Data augmentation for deep learning based semantic segmentation and crop-weed classification in agricultural robotics. *Computers and Electronics in Agriculture* **190**, 106418 (2021).

244. Rusin, D., Alehina, A., Safonova, A. & Dmitriev, E. Using deep learning algorithms for texture segmentation of ultra-high resolution satellite images. *E3S Web Conf.* **333**, 01010 (2021).

245. Li, Q. *et al.* Unsupervised Hyperspectral Image Change Detection via Deep Learning Self-Generated Credible Labels. *IEEE Journal of Selected Topics in Applied Earth Observations and Remote Sensing* **14**, 9012–9024 (2021).

246. Wang, Y., Cheng, J., Zhou, Y., Zhang, F. & Yin, Q. A Multichannel Fusion Convolutional Neural Network Based on Scattering Mechanism for PolSAR Image Classification. *IEEE Geoscience and Remote Sensing Letters* **19**, 1–5 (2022).

247. Jia, S. *et al.* A Lightweight Convolutional Neural Network for Hyperspectral Image Classification. *IEEE Transactions on Geoscience and Remote Sensing* **59**, 4150–4163 (2021).

248. Korznikov, K. A. *et al.* Using U-Net-Like Deep Convolutional Neural Networks for Precise Tree Recognition in Very High Resolution RGB (Red, Green, Blue) Satellite Images. *Forests* **12**, 66 (2021).

249. Wang, W., Liu, X. & Mou, X. Data Augmentation and Spectral Structure Features for Limited Samples Hyperspectral Classification. *Remote Sensing* **13**, 547 (2021).

250. Anna E. Alyokhina, Dmitry S. Rusin, Egor V. Dmitriev, & Anastasiia N. Safonova. Neural network texture segmentation of satellite images of woodlands using the U-net model. in 15–22 (CEUR Workshop Proceedings, 2021).

251. Alshammari, H. H. & Shahin, O. R. An Efficient Deep Learning Mechanism for the Recognition of Olive Trees in Jouf Region. *Computational Intelligence and Neuroscience* **2022**, e9249530 (2022).

252. Mitra, A., Mohanty, S. P. & Kougianos, E. A Smart Agriculture Framework to Automatically Track the Spread of Plant Diseases Using Mask Region-Based Convolutional Neural Network. in *Internet of Things. IoT through a Multi-disciplinary Perspective* (eds. Camarinha-Matos, L. M., Ribeiro, L. & Strous, L.) 68–85 (Springer International Publishing, 2022). doi:10.1007/978-3-031-18872-5_5.

253. Su, Z., Wang, Y., Xu, Q., Gao, R. & Kong, Q. LodgeNet: Improved rice lodging recognition using semantic segmentation of UAV high-resolution remote sensing images. *Computers and Electronics in Agriculture* **196**, 106873 (2022).

254. Momeny, M. *et al.* Detection of citrus black spot disease and ripeness level in orange fruit using learning-to-augment incorporated deep networks. *Ecological Informatics* **71**, 101829 (2022).

255. Mei, S. *et al.* Remote Sensing Scene Classification Using Sparse Representation-Based Framework With Deep Feature Fusion. *IEEE Journal of Selected Topics in Applied Earth Observations and Remote Sensing* **14**, 5867–5878 (2021).
256. Hua, W., Zhang, C., Xie, W. & Jin, X. Polarimetric SAR Image Classification Based on Ensemble Dual-Branch CNN and Superpixel Algorithm. *IEEE Journal of Selected Topics in Applied Earth Observations and Remote Sensing* **15**, 2759–2772 (2022).
257. Li, Q. *et al.* Construction of a small sample dataset and identification of Pitaya trees (Selenicereus) based on UAV image on close-range acquisition. *JARS* **16**, 024502 (2022).
258. Li, C., Liu, L., Zhao, J. & Liu, X. LF-CNN: Deep Learning-Guided Small Sample Target Detection for Remote Sensing Classification. *CMES* **131**, 429–444 (2022).
259. Huang, J. *et al.* Accurate Identification of Pine Wood Nematode Disease with a Deep Convolution Neural Network. *Remote Sensing* **14**, 913 (2022).
260. Chen, H., Fu, X. & Dong, J. SAR Target Recognition Based on Inception and Fully Convolutional Neural Network Combining Amplitude Domain Multiplicative Filtering Method. *Remote Sensing* **14**, 5718 (2022).
261. Liu, B. *et al.* Tree Species Classification Using Ground-Based LiDAR Data by Various Point Cloud Deep Learning Methods. *Remote Sensing* **14**, 5733 (2022).
262. Amarasingam, N., Gonzalez, F., Salgadoe, A. S. A., Sandino, J. & Powell, K. Detection of White Leaf Disease in Sugarcane Crops Using UAV-Derived RGB Imagery with Existing Deep Learning Models. *Remote Sensing* **14**, 6137 (2022).
263. Łopucki, R., Klich, D. & Kociuba, P. Detection of spatial avoidance between sousliks and moles by combining field observations, remote sensing and deep learning techniques. *Sci Rep* **12**, 8264 (2022).

Abbreviations

The following abbreviations or terms are used in this review paper:

RS	Remote Sensing
AI	Artificial Intelligence
ML	Machine Learning
DL	Deep Learning
CNN	Convolutional Neural Network
TL	Transfer Learning
NLP	Natural Language Processing
HSI	Hyperspectral Imaging
UAV	Unmanned Aerial Vehicle

Acknowledgments This study was supported by the Federal Ministry of Education and Research (BMBF – Bundesministerium für Bildung und Forschung) project “Multi-modale Datenintegration, domänenspezifische Methoden und KI zur Stärkung der Datenkompetenz in der Agrarforschung” (16DKWN089). We thank Sebastian Raschka for offering valuable feedback.

Competing interests The authors declare no competing interests.

Appendix A. List of publications with detailed information

No.	Reference	Type of DL task	Classes and object of study	Dataset and images
1	Dyrmann et al. (ref.[41])	Classification	22 classes: weed and crop species	6 datasets with 5,539, 1,630, 1,447, 745, 284, and 62 images
2	dos Santos Ferreira et al. (ref.[228])	Detection	4 classes: soil, soybean, grass, and broadleaf	2 datasets taken from DJI Phantom 3 Professional UAV with Sony EXMOR 1/2.3″ RGB camera, 4500 images
3	Liu and Zheng (ref.[33])	Classification	7 classes: military ships as BMP-2(9563), BMP-2(9566), BMP-2(c21), BTR-70(c71), T-21(132), T-21(812), and T-21(s7) 5 classes: destroyers, aircraft carriers, oil tankers, bulk carriers, container ships	2 datasets: moving and stationary target acquisition and recognition (MSTAR) dataset gathered from the X-band (9.6 GHz) HH-polaridation SAR sensor with the resolution of 0.3 m × 0.3 m, 1,365 images, and high-resolution ship target classification and recognition (HSTCR) from Google Earth, 500 images
4	Cicco et al. (ref.[229])	Semantic segmentation	2 classes: beets and weeds, including sugar beet plants, *Capsella Bursa-Pastoris* weed, and *Galium Aparine* weed	2 real datasets taken from BOSCH Bonirob farm robot with 4 channels (RGB-NIR) JAI AD-130 with 700 and 900 samples, and 4 synthetic datasets, each composed of 1,300 images
5	Guirado et al. (ref.[42])	Detection	2 classes: *Ziziphus* lotus shrubs and bare soil	Dataset extracted from Google Earth™ (WorldView-2 and y Pléiades-1A satellites), 200 images, with 100 images per class
6	Fuentes et al. (ref.[230])	Detection	10 classes: tomato plant diseases and pests, including leaf mould, grey	Dataset collected from farms using simple camera devices, 5,000

			mould, canker, plague, miner, low temperature, powdery mildew, whitefly, nutritional excess, and background	images
7	Zhou et al. (ref.[231])	Classification	3 classes: leaf litter with low coverage, leaf litter with high coverage, and leaves	Dataset from UAV with a Canon EOS 1000D camera, 8,112 images with a size of 50 × 50 pixels
8	Chew et al. (ref.[232])	Classification	2 classes: “residential” or “nonresidential” areas	2 datasets: Crowdsourced geospatial features from OpenStreetMaps and remotely sensed features from the European Space Agency (ESA) Land Cover dataset. Nigeria – 5,350 images and Guatemala – 1,500 images
9	Kang et al. (ref.[80])	Classification	16 classes: Indian Pines dataset – alfalfa, corn-no till, corn-min till, corn, grass-pasture, grass-trees, grass-pasture-mowed, hay-windrowed, oats, soybean-no till, soybean-min till, soybean-clean, wheat, woods, building-grass-trees-drives, and stone-steel-towers 9 classes: University of Pavia dataset – asphalt, meadows, gravel, trees, painted metal, sheets, bare soil, bitumen, self-blocking, bricks, and shadows	2 datasets: hyperspectral images (HSIs): Indian Pines (IP) image, which was acquired by the Airborne Visible Infrared Imaging Spectrometer (AVIRIS), spatial size of 145 × 145 pixels and 200 bands with 20 m spatial resolution and University of Pavia (UP) image, which was acquired by the reflective optics system imaging spectrometer (ROSIS-03) optical sensor, a spatial size of 610 × 340 pixels and 103 bands with 1.3 m spatial resolution
10	Safonova et al. (ref.[36])	Detection	4 classes: Fir trees as completely healthy trees or trees recently attacked by beetles, trees colonised	Dataset from UAV DJI Phantom 3 Pro, 200 images

			by beetles, trees that had recently died and deadwood	
11	Windrim et al. (ref.[39])	Detection	3 classes: stump, different size classes of debris (CWD versus FWD)	Dataset from AscTec Falcon-8 UAV, 1,000 images
12	Freeman et al. (ref.[30])	Detection	6 classes: Buddleia, Cornus, Hydrangea paniculata, Hydrangea quercifolia, Physocarpus, Spiraea	Near-infrared images were previously collected using modified Canon and MAPIR Survey II cameras deployed via a small unmanned aircraft system (sUAS) at an altitude of 30 metres, 150 images
13	Malambo et al. (ref.[34])	Semantic segmentation	3 classes: Panicle, for all panicle instances in an image; Ground, for exposed ground surfaces in the image and; Background, for green foliage and any shadowed regions	Dataset from unmanned aerial system (UAS), 462 images
14	Barbedo et al. (ref.[233])	Classification	Cattle	UAV DJI Phantom 4 Pro, equipped with a 20-MPixel camera, 1,853 images
15	Wu et al. (ref.[76])	Classification	16 classes: Indian Pines dataset – alfalfa, corn-no till, corn-min till, corn, grass-pasture, grass-trees, grass-pasture-mowed, hay-windrowed, oats, soybean-no till, soybean-min till, soybean-clean, wheat, woods, building-grass-trees-drives, and stone-steel-towers 16 classes: Salinas dataset – broccoli-green-weeds-1, broccoli-green-weeds-2, fallow, fallow-rough-plow, fallow-smooth, stubble, celery, grapes-untrained, soil-vineyard-develop, corn-senesced-	3 hyperspectral remote sensing (HSI) images: UP dataset was acquired by the Reflective Optics System Imaging Spectrometer (ROSIS) sensor, 610 × 340 pixels and 103 spectral bands; Salinas (SA) dataset collected by the Airborne Visible/Infrared Imaging Spectrometer (AVIRIS) sensor, 512 × 217 pixels and 204 spectral bands; IP dataset, gathered by

			green-weeds, lettuce-romaine-4wk, lettuce-romaine-5wk, lettuce-romaine-6wk, lettuce-romaine-7wk, vineyard-untrained, and vineyard-vertical-trellis 9 classes: University of Pavia dataset – asphalt, meadows, gravel, trees, painted metal, sheets, bare soil, bitumen, self-blocking, bricks, and shadows	AVIRIS sensor, 145 × 145 pixels and 200 spectral bands
16	Pang et al. (ref.[43])	Segmentation	Maize stand	UAV, Quadrotor UAV platform – DJI Inspire 1, Micasense RedEdge camera, 100 patches
17	Xue et al. (ref.[234])	Classification	45 classes: AID dataset - airport, bare land, baseball field, beach, bridge, center, church, commercial, high-density residential, desert and others; NWPU-RESISC45 dataset – airplane, airport, baseball diamond, basketball court, beach, bridge, chaparral, church, circular farmland, cloud and others; UC Merced dataset – agricultural airplane, baseball diamond, beach, buildings, chaparral, high-density residential, forest, freeway, golf course and others	3 datasets: UC Merced (aerial imagery), 2,100 images; AID (Google Earth), 10,000 images; NWPU-RESISC45 (Google Earth) datasets, 31,500 images
18	Wang et al. (ref.[75])	Classification	16 classes: Indian Pines dataset – alfalfa, corn-no till, corn-min till, corn, grass-pasture, grass-trees, grass-pasture-mowed, hay-windrowed, oats, soybean-no till, soybean-min till, soybean-clean, wheat, woods, building-grass-trees-drives, and	3 HSI images: IP dataset, gathered by AVIRIS sensor, 145 × 145 pixels and 100 spectral bands; UP dataset was acquired by the Reflective Optics System Imaging Spectrometer (ROSIS)

			stone-steel-towers 16 classes: Salinas dataset – broccoli-green-weeds-1, broccoli-green-weeds-2, fallow, fallow-rough-plow, fallow-smooth, stubble, celery, grapes-untrained, soil-vineyard-develop, corn-senesced-green-weeds, lettuce-romaine-4wk, lettuce-romaine-5wk, lettuce-romaine-6wk, lettuce-romaine-7wk, vineyard-untrained, and vineyard-vertical-trellis 9 classes: University of Pavia dataset – asphalt, meadows, gravel, trees, painted metal, sheets, bare soil, bitumen, self-blocking, bricks, and shadows	sensor, 610 × 340 pixels and 50 spectral bands; SA dataset collected by the Airborne Visible/Infrared Imaging Spectrometer (AVIRIS) sensor, 512 × 217 pixels and 29 spectral bands
19	Blekos et al. (ref.[29])	Segmentation	Trees: Birch (*Betula ptula platyphylla Suk.*), Larch (*Larix gmelinii Rupr*.), Locust (*Styphnolobium japonicum L.*), Willow (*Salix babylonica L.*), Poplar (*Populus L.*), Elm (*Ulmuspumila L.*), Eucalyptus (*Eucalyptus robust Sm.*), Chinese fir (*Cunninghamia lanceolata (Lamb.) Hook.*)	Dataset from UAV with Pix4d Parrot Sequoia camera, 400 images
20	Zhang et al. (ref.[235])	Classification	10 classes: MSTAR dataset of vehicles as 2S1, D7, T62, BRDM, ZIL131, ZSU234, BMP2, BTR70, BTR60, T72	MSTAR dataset from SAR images
21	Li et al. (ref.[236])	Classification	21 classes: land use classes as agriculture, airplane, beach, buildings, forest, river and others	3 datasets: UC Merced land use (UCM), 100 images with a resolution of 250 × 250 pixels; WHU-RS19, 19 categories of images with approximately 50

				samples, 256 × 256 pixels; Google image dataset of WHU-RS19, 200 images of the same size of 200 × 200 pixels
22	Zhou et al. (ref.[237])	Recognition	10 classes: MSTAR dataset of vehicles as 2S1, D7, T62, BRDM, ZIL131, ZSU234, BMP2, BTR70, BTR60, T72	The MSTAR public dataset collected by the X-band SAR automatic target recognition (SAR-ATR) sensor, 2,425 images
23	Han et al. (ref.[238])	Classification	3 classes: white ice, grey ice, and seawater 4 classes: white ice, grey white ice, grey ice, and seawater 3 classes: white ice, grey ice, and seawater	3 datasets of HSI: Baffin Bay image captured by Earth Observing-1 (EO-1) satellite, 176 bands; Bohai Bay image captured by EO-1 satellite, 1,247 samples; Liaodong Bay image captured by Landsat-8 satellite, 1 image
24	Chew et al. (ref.[239])	Detection	6 classes: banana, maize, legume, forest, structure and other	Dataset from eBee Plus UAV with senseFly S.O.D.A. camera, 6,470 images
25	Liu et al. (ref.[240])	Classification	13 classes: impervious surfaces, buildings, low vegetation, trees, cars, clutter/background, farmland, forestland, bare soil, building area, water, road, artificial structures	2 datasets: ISPRS 2D semantic labelling contest of Vaihingen, 33 images; Shanghai dataset, 6 images
26	Tian et al. (ref.[241])	Classification	11 classes: forest species as *M. Laosensis*, *P.elliotti*, *P. massoniana*, *E. urophylla*, *E. grandis*, *C. hystrix*, *A. Meloxylon*, *M. laosensis*, soft broadleaf, cutting site, and road	HSI dataset was housed in a LiCHy system that integrates light detection and ranging (LiDAR), a charge-coupled device camera, an AISA Eagle II hyperspectral sensor, and an inertial measurement unit (IMU), 125 bands
27	He et al.	Detection	Wheat plant	Global Wheat Head

	(ref.[242])			Detection (GWHD) dataset, 4,700 images
28	Chen et al. (ref.[118])	Detection	Aircraft	DOTA dataset, 5,716 images
29	Su et al. (ref.[243])	Semantic segmentation	2 classes: crops and weeds	2 datasets: Narrabri and Bonn from the wheat farm (4-channel RGB + NIR camera JAI AD-130 GE), 283 and 150 images
30	Kato et al. (ref.[81])	Classification	8 classes: volcano, factory, oil platform, fire (grass), fire (forest), fire (urban), specular reflection, non-typeable	Landsat 8 OLI (11 bands) and Thermal Infrared Sensor (TIRS) and Sentinel-2 MSI (12 bands), 2,516 images
31	Rusin et al. (ref.[244])	Segmentation	6 classes: mixed forest, field, city, forest belt, ordered forest, water	Dataset from WorldView-2 satellite 1,267 × 1,265, 64 parts
32	Gao et al. (ref.[79])	Classification	9 classes: University of Pavia dataset – asphalt, meadows, gravel, trees, painted metal, sheets, bare soil, bitumen, self-blocking, bricks, and shadows 16 classes: Salinas dataset – broccoli-green-weeds-1, broccoli-green-weeds-2, fallow, fallow-rough-plow, fallow-smooth, stubble, celery, grapes-untrained, soil-vineyard-develop, corn-senesced-green-weeds, lettuce-romaine-4wk, lettuce-romaine-5wk, lettuce-romaine-6wk, lettuce-romaine-7wk, vineyard-untrained, and vineyard-vertical-trellis 13 classes: KSC dataset – scrub, willow swamp, CP hammock, slash pine, oak/broadleaf, hardwood, swamp, graminoid marsh, cattail marsh, salt marsh,	3 HSI datasets: UP, ROSIS, 610 × 340 pixels with 103 bands; (SA), AVIRIS, 512 × 217 pixels with 204 bands; Kennedy Space Centre (KSC), AVIRIS, 512 × 614 pixels with 176 bands

			mud flats, and water	
33	Zuo et al. (ref.[78])	Classification	9 classes: University of Pavia dataset -– asphalt, meadows, gravel, trees, painted metal, sheets, bare soil, bitumen, self-blocking, bricks, and shadows 16 classes: Salinas dataset – broccoli-green-weeds-1, broccoli-green-weeds-2, fallow, fallow-rough-plow, fallow-smooth, stubble, celery, grapes-untrained, soil-vineyard-develop, corn-senesced-green-weeds, lettuce-romaine-4wk, lettuce-romaine-5wk, lettuce-romaine-6wk, lettuce-romaine-7wk, vineyard-untrained, and vineyard-vertical-trellis 9 classes: Pavia center dataset – water, trees, meadow, brick, bare soil, asphalt, bitumen, tile, shadows	3 HSI datasets: UP, ROSIS, 610 × 340 pixels with 103 bands; SA, AVIRIS, 512 × 217 pixels with 224 bands; Pavia Center (PC), 1,096 × 715 pixels with 102 bands
34	Gao et al. (ref.[74])	Segmentation	3 classes: beach, island, sea ice	NWPU-RESISC45 dataset
35	Safonova et al. (ref.[37])	Detection	4 classes: Norway Spruce Trees (*Picea Abies*) attacked by the European bark beetle – green, yellow, red, and grey attack	Dataset from DJI-Phantom 4 Pro UAV, 400 images
36	Khan et al. (ref.[91])	Semantic segmentation	5 classes: corn, soybean, winter wheat, alfalfa hay, and others	Dataset of Landsat 8 from USGS and NASA with OLI/TIRS sensors, 7 bands, 2015–2019
37	Li et al. (ref.[245])	Segmentation	2 classes: farmland and river	2 datasets are from earth observing-1 (EO-1) hyperion hyperspectral sensor, 3 images for one dataset
38	Astolfi et al.	Classification	4 classes: weeds, disease	Dataset from UAV DJI

	(ref.[57])		soybean, healthy soybean, and soil	Phantom 3 Pro with an integrated Sony EXMOR 1/2.3" camera, 400 images
39	Wang et al. (ref.[246])	Classification	15 classes: steam bean, rapeseed, bare soil, potatoes, wheat, wheat-2, peas, wheat-3, lucerne, barley, grasses, beets, buildings, water, and forest 8 classes: bare, forest, cole, wheat, grass, water, sand, wetland	2 datasets from airborne synthetic aperture radar (AIRSAR) Flevoland data and GF-3 data, Polarimetric Synthetic Aperture Radar (PolSAR) images
40	Jia et al. (ref.[247])	Classification	16 classes: Indian Pines dataset – alfalfa, corn-no till, corn-min till, corn, grass-pasture, grass-trees, grass-pasture-mowed, hay-windrowed, oats, soybean-no till, soybean-min till, soybean-clean, wheat, woods, building-grass-trees-drives, and stone-steel-towers 16 classes: Salinas dataset – broccoli-green-weeds-1, broccoli-green-weeds-2, fallow, fallow-rough-plow, fallow-smooth, stubble, celery, grapes-untrained, soil-vineyard-develop, corn-senesced-green-weeds, lettuce-romaine-4wk, lettuce-romaine-5wk, lettuce-romaine-6wk, lettuce-romaine-7wk, vineyard-untrained, and vineyard-vertical-trellis 9 classes: University of Pavia dataset – asphalt, meadows, gravel, trees, painted metal, sheets, bare soil, bitumen, self-blocking, bricks, and shadows	3 datasets: IP, SA, and UP
41	Korznikov et	Segmentation	3 classes: poplar trees,	Image from GeoEye-1

	al. (ref.[248])		coniferous trees, and background	satellite
42	Zhao et al. (ref.[117])	Detection	Crop detection	Dataset from Zenmuse-X4S camera-equipped DJI-Inspire-2, 243 and 100 images
43	Wang et al. (ref.[249])	Classification	16 classes: Indian Pines dataset – alfalfa, corn-no till, corn-min till, corn, grass-pasture, grass-trees, grass-pasture-mowed, hay-windrowed, oats, soybean-no till, soybean-min till, soybean-clean, wheat, woods, building-grass-trees-drives, and stone-steel-towers 9 classes: University of Pavia dataset – asphalt, meadows, gravel, trees, painted metal, sheets, bare soil, bitumen, self-blocking, bricks, and shadows	2 HSI datasets: IP and UP
44	Jozdani et al. (ref.[157])	Classification	Caribou lichen	Dataset from DJI Inspire-1 UAV and 8-band WorldView scene, 1,825 samples
45	Safonova et al. (ref.[37])	Semantic segmentation	2 classes: olive tree and its shadow	Dataset from Parrot Disco-Pro AG UAV and DJI-Phantom 4 UAV, 600 images
46	Naushad et al. (ref.[120])	Classification	10 classes: forest, annual crop, highway, herbaceous vegetation, pasture, residential, river, industrial, permanent crop, and sea/lake	MSI EuroSAT dataset from Sentinel-2 satellite, 13 spectral bands consisting of 27,000 labelled and georeferenced images, with 2,000–3,000 images per class
47	Alyokhina et al. (ref.[250])	Segmentation	7 classes: coniferous tree (high density), field 1, field 2, mixed wood (high density), cluster mixed forest, mixed wood (medium density), and	Image from WorldView-2

			common larch	
48	Barbosa et al. (ref.[90])	Classification	Coffee tree	Dataset from DJI Phantom 3 with a Sony IMX147 camera, 144 samples
49	Alshammari and Shahin (ref.[251])	Segmentation	Olive Tree	Dataset from Parrot DiscoPro AG UAV and DJI-Phantom 4 UAV, 600 images
50	Mitra et al. (ref.[252])	Detection	Leaf diseases in *Black Rot*, *Apple Scab*, and *Cedar Apple Rust*	Dataset from smart phone and UAV, 850 images
51	Su et al. (ref.[253])	Segmentation	6 classes: root lodging rice, stem lodging rice, normal rice, building, tree, and background	Dataset from DJI Phantom 4 Pro UAV with a DJI FC6310 camera, 4,000 × 3,000 pixels, 25,920 cropped images
52	Momeny et al. (ref.[254])	Detection	4 classes: unripe, half-ripe, ripe, and infected with black spot disease (citrus and orange)	Dataset from a Samsung SM-J500H smartphone camera, 1,896 images
53	Ho et al. (ref.[58])	Classification	5 classes as crown loss bins (0–20% (healthy tree), 20–40%, 40–60%, 60–80% and 80–100% (dead trees)), ash, fir, oak, birch	WSL dataset from a virtual camera
54	Shin et al. (ref.[83])	Classification	2 classes: Harmful algal bloom (HAB) and non-HAB	OLCI imagery on board from Sentinel-3A and 3B, 16 bands, 21 images of 10,987 samples
55	Sapkota et al. (ref.[44])	Detection	Weed, as a mix of morning glories (*Ipomoea* spp.) that comprised of tall morning glory [*Ipomoea purpurea* (L.) Roth.] and ivyleaf morning glory (*Ipomoea hederacea* Jacq.), Texas millet [*Urochloa texana* (Buckley) R.D. Webster], and johnsongrass [*Sorghum halepense* (L.)	2 datasets: Cotton 1 from Hylio AG-110 multi-copter drone with 100-megapixel FUJIFILM GFX100 RGB camera, 560 images; Cotton 2 from drone with a FUJIFILM GF 32–64 camera, 100 images

			Pers.], Palmer amaranth (*Amaranthus palmeri* S. Watson), prostrate spurge (*Euphorbia humistrata* Engelm.), and browntop panicum (*Panicum fasiculatum* Sw.)	
56	Mei et al. (ref.[255])	Classification	21 classes: agricultural, airplane, baseball diamond, beach, buildings, chaparral, dense residential, forest, freeway, golf course, harbour, intersection, medium-density residential, mobile home park, overpass, parking lot, river, runway, sparse residential, storage tanks, and tennis courts; 19 classes: airport, beach, bridge, commercial, desert, farmland, football field, forest, industrial, meadow, mountain, park, parking, pond, port, railway station, residential, river, viaduct	2 datasets: UC-Meced21 from the USGS National Map Urban Area Imagery collection with 100 images per class; WHU-RS19 by Wuhan University with 50 images per class
57	Hua et al. (ref.[256])	Classification	15 classes: stem, rapeseed, bare soil, potatoes, beet, wheat-2, peas, wheat-3, lucerne, barley, wheat, grasses, forest, water, building	2 PolSAR datasets: AIRSAR (750 × 1024 pixel, 10 samples) and RADARSAT-2 data (1,400 × 1,200 pixels, 40 samples)
58	Li et al. (ref.[32])	Classification	10 classes: airplane, ship, storage tank, baseball field, tennis court, basketball court, ground track, field, harbour, bridge, and vehicle	2 datasets: NWPU VHR-10 with a few samples and part of DIOR (900 images)
59	Wang et al. (ref.[89])	Segmentation	Wheat ears	2 datasets: Wheat-ear semantic segmentation dataset (WESS-D), 160 images for training, 60 – for testing;

				Wheat-ear counting dataset (WEC-D), 6500 sub-images
60	Xu et al. (ref.[77])	Classification	16 classes: Indian Pines dataset – alfalfa, corn-no till, corn-min till, corn, grass-pasture, grass-trees, grass-pasture-mowed, hay-windrowed, oats, soybean-no till, soybean-min till, soybean-clean, wheat, woods, building-grass-trees-drives, and stone-steel-towers 9 classes: University of Pavia dataset – asphalt, meadows, gravel, trees, painted metal, sheets, bare soil, bitumen, self-blocking, bricks, and shadows 13 classes: KSC dataset – scrub, willow swamp, CP hammock, slash pine, oak/broadleaf, hardwood, swamp, graminoid marsh, cattail marsh, salt marsh, mud flats, and water	3 datasets: IP, UP, and KSC
61	Xue et al. (ref.[60])	Classification	16 classes: Salinas dataset – broccoli-green-weeds-1, broccoli-green-weeds-2, fallow, fallow-rough-plow, fallow-smooth, stubble, celery, grapes-untrained, soil-vineyard-develop, corn-senesced-green-weeds, lettuce-romaine-4wk, lettuce-romaine-5wk, lettuce-romaine-6wk, lettuce-romaine-7wk, vineyard-untrained, and vineyard-vertical-trellis 9 classes: University of Pavia dataset – asphalt, meadows, gravel, trees, painted metal, sheets, bare soil, bitumen, self-blocking, bricks, and	4 datasets: SA, UP, Trento from LiDAR with 63 bands, Houston 2018 datasets (HU) and VHR dataset with 48 bands

			shadows 6 classes: Trento dataset – apple trees, buildings, ground, wood, vineyard, and roads 20 classes: healthy grass, deciduous tree, non-residential building, major thoroughfare, unpaved parking lot, stressed grass, bare earth, road, highway, car, artificial turf, sidewalk, railway, train, artificial turf, water, sidewalk, railway, train, evergreen tree, residential building, crosswalk, paved parking lot, and stadium seat	
62	Li et al. (ref.[257])	Segmentation	5 classes: Pitaya trees (*Selenicereus*), twining vines, weed and tree cover, blurred images, and shadows	Dataset from DJI Mavic 2 Pro UAV, from 200 to 21,593 samples
63	Li et al. (ref.[258])	Classification	6 classes: RS target corresponding to 6 categories of land cover	HSI images with 68, 41, and 99 bands, taken from satellite-borne sensors
64	Wang et al. (ref.[116])	Classification	6 classes: 3 kinds of weeds and 3 crops as *Chenopodium album*, *Humulus scandens*, maize, peanut seedlings, wheat, *Xanthium sibiricum* Patrin ex Widder	DJI M100 with a ZENMUSE 100 camera, DJI Phantom 3 Pro with Red Edge, 2 metres, 3,266 images
65	Zenkl et al. (ref.[40])	Classification	2 classes: winter wheat plants of 76 different genotypes and developmental stages and soil	Dataset from a Canon 5D Mark II full-frame RGB camera, 190 images
66	Liu et al. (ref.[45])	Segmentation	5 classes: river, lake, sea, meadow, forest textures	Dataset NWPU-RESISC45, 700 images
67	Xue et al. (ref.[82])	Classification	Forest fire	Dataset from long-range photography of forest fires, UAV, and initial forest fire photos,

				3,320 images
68	Fend et al. (ref.[59])	Classification	16 classes: Indian Pines dataset – alfalfa, corn-no till, corn-min till, corn, grass-pasture, grass-trees, grass-pasture-mowed, hay-windrowed, oats, soybean-no till, soybean-min till, soybean-clean, wheat, woods, building-grass-trees-drives, and stone-steel-towers 15 classes: Houston dataset – grass healthy, grass stressed, grass synthetic, tree, soil, water, residential, commercial, road, highway, railway, parking lot 1, parking lot 2, tennis court, and running track 9 classes: University of Pavia dataset – asphalt, meadows, gravel, trees, painted metal, sheets, bare soil, bitumen, self-blocking, bricks, and shadows	3 HSI datasets: IP, HU, and PU
69	Reedha et al. (ref.[87])	Classification	5 classes: weeds, beet, off-type green leaves beet, parsley, and spinach	Dataset from Stratify UAV with a Sony ILCE-7R camera, 4000 images
70	Zhang et al. (ref.[184])	Segmentation	8 classes: tree species as *Pinus armandii*, *Ginkgo biloba*, *Pinus tabulaeformis*, *Sophora japonica*, *Salix matsudana*, *Ailanthus altissima*, *Amygdalus davidiana*, and *Populus nigra*	Dataset from UAV, 1,029 patch images
71	Huang et al. (ref.[259])	Classification	Pine Wood Nematode Disease	Dataset from China's Gaofen-1 (GF-1) and Gaofen-2 (GF-2), 3,570 images
72	Ding et al. (ref.[73])	Classification	9 classes: University of Pavia dataset – asphalt,	3 HSI datasets: UP, SA, and IP

			meadows, gravel, trees, painted metal, sheets, bare soil, bitumen, self-blocking, bricks, and shadows 16 classes: Salinas dataset – broccoli-green-weeds-1, broccoli-green-weeds-2, fallow, fallow-rough-plow, fallow-smooth, stubble, celery, grapes-untrained, soil-vineyard-develop, corn-senesced-green-weeds, lettuce-romaine-4wk, lettuce-romaine-5wk, lettuce-romaine-6wk, lettuce-romaine-7wk, vineyard-untrained, and vineyard-vertical-trellis 16 classes: Indian Pines dataset – alfalfa, corn-no till, corn-min till, corn, grass-pasture, grass-trees, grass-pasture-mowed, hay-windrowed, oats, soybean-no till, soybean-min till, soybean-clean, wheat, woods, building-grass-trees-drives, and stone-steel-towers	
73	Yu et al. (ref.[88])	Segmentation	2 classes: terraces on the Loess Plateau and non-terraced fields	Dataset from WorldView-1 (17760 images) and GF-2 satellite (1,300 images) RS image data
74	Li et al. (ref.[63])	Classification	3 classes: non-farmland, winter wheat, and garlic	Dataset from RadarSat-2 C-band full polarimetric SAR, 5 images
75	Chen et al. (ref.[260])	Classification	10 classes: MSTAR dataset of vehicles as 2S1, D7, T62, BRDM, ZIL131, ZSU234, BMP2, BTR70, BTR60, T72	Moving and Stationary Target Acquisition and Recognition (MSTAR) dataset
76	Liu et al (ref.[261])	Classification	8 classes: trees as Birst (*Betula ptula platyphylla* Suk.), Larch (*Larix*	LiDAR data – a LiBackpack DGC50 backpack laser

			gmelinii Rupr.), Locust (*Styphnolobium japonicum* L.), Willow (*Salix babylonica* L.), Poplar (*Populus* L.), Elm (*Ulmuspumila* L.), Eucalyptus (*Eucalyptus robust* Sm.), Chinese fir (*Cunninghamia lanceolata* (Lamb.) Hook.)	scanning (BLS) system from Beijing GreenValley Technology Co., Ltd. with the LiBackpack DGC50 system
77	Amarasingam et al. (ref.[262])	Detection	White leaf disease in sugarcane crops	Dataset from DJI Phantom 4 UAV, 1,440 images
78	Łopucki et al. (ref.[263])	Detection	2 classes: souslik Spermophilus suslicus and the European mole Talpa European	Orthoimagery dataset from GUGiK (Google Earth), 1,987 images
79	Putra and Wijayanto (ref.[35])	Detection	Oil palm trees	Dataset from Microsoft Bing Maps Very High Resolution (VHR) satellite imagery and UAV with image, 507 images
80	Hong-Yu et al. (ref.[31])	Detection	Ramie Plant	3 datasets from Inspire 2 UAV, 177, 235, and 531 samples

Continuation of Appendix A. List of publications with detailed information

No.	Data augmentation	DL algorithm	Performance metric	Value of the metric	Application
1	Mirroring and rotating in 90°	Proposed CNN	CA	1: 65%–93% 2: 91% 3: 94.8% 4: 95.8% 5: 99% 6: 82.4%–88.2% CA: 86.20%	Theano-based Lasagne library
2	Cropping a large image into small patches by the Pynovisão software with the SLIC algorithm	CaffeNet	P, S	1: 98% 2: 99.5%	Caffe framework for DL implemented in C++/CUDA
3	Proposed target classification and recognition (TCR) of Incremental Reinforcement and Ensemble Learning based on the Object-Oriented and Multi-Scale data augmentation (TCR-IREL-OOMS) algorithm according to TCR-IEL-OOTDA algorithm, and TCR-REL-MSTDA algorithm	TCR-EL-DHMM algorithm, linear SVM, Kernel SVM, SRCA, SRC, NMF+SVM, DBN, HRS	OA, P	1: P – 100%, AO – 100% 2: P – 96.93%, AO – 97.00%	N/A
4	Composing a dataset by adding images from other datasets, image resize to 480 by 360 pixels and randomising the key features of the target environment	SegNet	AA	AA – 91.30%	N/A
5	Transfer learning (TL), data augmentation as random scale, random crop, flip	ResNet and GoogLeNet	P, R, F1	P – 100%, R – 93.24%, F1 – 96.5%	TensorFlow

	horizontally, random brightness				
6	Geometrical transformations (resizing, crop, rotation, horizontal flipping) and intensity transformations (contrast and brightness enhancement, colour, noise)	Faster Region-based Convolutional Neural Network (Faster R-CNN), Region-based Fully Convolutional Network (R-FCN), and Single Shot Multibox Detector (SSD) with VGG and ResNet	IoU > 0.5, AP	Without DA: AP – 0.5564 With DA: AP – 0.8306	N/A
7	Cropping a large image into small patches	ResNet50, VGG16, and VGG19	CA	95.1%	N/A
8	Cropping a large image into small patches	VGG16 with ImageNet weights, InceptionV3 with ImageNet weights, VGG16 and InceptionV3 ensemble, Decision Tree, Gradient Boosting, AdaBoost, Random forest, Logistic regression, Support vector machine, K-nearest neighbours, Human benchmark	OA, P, R, F1	1: OA for Nigeria – 94.5% 2: OA for Guatemala – 96.4%	Keras, Scikit-learn
9	Combining original training samples and high-confidence samples which are acquired by performing decision fusion on the classification probabilities	Deep feature fusion network (DFFN)	OA, AA, *k*	1: OA – 95.14%, AA – 93.97%, *k* – 94.46% 2: OA – 97.41%, 97.2%, *k* – 96.58% 3: OA – 95.14%, AA – 93.97%, *k* – 94.46%	Caffe framework for DL in C++/CUDA
10	Rotation and translation to the original samples	Proposed CNN, Xception, VGG16, VGG19, ResNet50, Inception V3, InceptionResNetV2, DenseNet121, DenseNet169 and	OA, P, R, F1	OA – 98.77%	TensorFlow, Keras

		DenseNet201			
11	Rotation and flip to balance classes and make the CNN more generalisable	Faster R-CNN	IoU, P, R	P – 0.939 ± 0.112, R – 0.818 ± 0.85	TensorFlow 1.4.1
12	N/A	Watson generated models	*p*-value	*p*-value < 0.05	Python
13	Randomly shifting, rotating, and reflecting	Adapted a SegNet	OA, IoU	OA – 95%, IoU – 87%	Computer vision using DL, Matlab
14	N/A	VGG-16, VGG-19, ResNet-50 v2, ResNet-101 v2, ResNet-152 v2, MobileNet, MobileNet v2, DenseNet 121, DenseNet 169, DenseNet 201, Xception, Inception v3, Inception ResNet v2, NASNet Mobile, NASNet Large	OA, P, R, F1	AO – 95%	Keras, TensorFlow v. 1.4.
15	N/A	ProCNN, AlexNet, VGGNet	OA, *k*	OA – up to 99.3%, *k* – up to 0.995	Image Processing Toolbox, Matlab
16	Besides, vertical and horizontal flipping, scaling outward by 10% and 20%, rotation, and Gaussian Noise	MaxArea Mask Scoring RCNN	AP	95.80%	Keras and TensorFlow
17	Random-scale cropping	SPCK, ResNet-101, GoogleLeNet, VGG-VD-16, Fine-tuned GoogleLeNet, Fine-tuned ResNet-50, Triplet-Stream Fusion, Deep CNN Transfer, PMS, Proposed methods	CA	Up to 99.76%	TensorFlow
18	N/A	Bidirectional Long Short-Term Memory (Bi-LSTM) and AlexNet, ResNet, DenseNet, PRAN, FSSFNet, SAGP, AML	OA, AA, *k*	OA – up to 93.92%, AA – up to 97.8% *k* – up to 96.66%	TensorFlow
19	N/A	U-net	AA	Up to 89%	Keras

20	3 main strategies: network structure, sample of feature augmentation, and ensemble learning strategies	CNN Cascaded Features and AdaBoost Rotation Forest	OA	Up to 96.30%	TensorFlow
21	N/A	VGG-16, InceptionV3, ResNet-50, ResNet-101	CA	UCM: 99% WHU-RS19: 98.8% SIRI_WHU: 96.1%	TensorFlow slim module for end-to-end learning
22	Regularisation methods, including rotation, translation, mirroring, random cropping, and adding noise	The limited data loss function (LDLF) supervises the CNN	AA	Up to 84.77%	N/A
23	N/A	3D-CNN and Squeeze-and-Excitation Networks: SVM, Siamese, CNN, CNN-SVM, SE-CNN-SVM	CA	94.58%, 95.11%, 97.42%	TensorFlow
24	Resizing, randometric corrections	VGG-16	F1, P, R, A, *k*	OA is 93% F1 is 90%	Python
25	Cropping into smaller patches of size 400 × 400 pixels, using a sliding window, then sliced into smaller size, further increasing and random vertical and horizontal flips	SVL-boosting + CRF, RF + dCRF, RotEqNet, HSNet, ENR, SegNet, MobileNet, FC-DenseNet, REMSNet	F1, OA, IoU, P	1: OA – 90.46%, IoU – 0.8073 2: OA – 88.55%, IoU – 0.7394	TensorFlow
26	Cropping a large image into small patches	IPrNet, 3D-CNN	OA, *k*	OA – 98.53% and 87.5%, *k* – 0.9838 and 0.8625	N/A
27	HSV channel colour conversion; Brightness and contrast conversion; Horizontal flip, vertical flip,	YOLOv4 (A), A + improved depthwise separable conv (B), B + modified network and anchors re-clustered byk-means (C), D + Adaptive	P, IoU	P is up to 98.46%	Darknet DL framework with Python 3.7

	greyscale conversion, and random cropping; Cutout method, and Mosaic method	ReLU (D), and D + method of prediction box fusion			
28	Rotation at 90°, 180°, and 270°	Domain Adaptation Faster R-CNN (DA Faster R-CNN)	AP	Up to 54.28%	N/A
29	RICAP data augmentation method with random flipping, rotation, and colour jitter	Novel data augmentation framework, based on the random image cropping and patching (RICAP) method	P, R, CA, IoU	IoU – from 91.01% to 98.51%	N/A
30	N/A	New CNN	CA	97.9%	N/A
31	Cropping a large image into small patches, DA as rotation, flipping left, right, up, and down	U-Net	P, R, F1, mAP	F1 – 82.37%, mAP – 76.49%	TensorFlow, Keras
32	N/A	RBF-SVM, 3D-CNN, SGAN, EMP+GCN, 3D-CAE, RN-FSC, DFSL+SVM, MAML-CNN	OA, AA, *k*	OA are 95.5%, 96.34%, 86.49% on UP, SA, KSC	N/A
33	N/A	SVM, LapSVM, TSVM, SCS^3VM, Res-3D-CNN, SS-CNN, Graphsage, and LBP+Graphsage	OA	81.20±0.41 for UP, 85.22±0.68 for SA, 97.61±0.31 for PC	N/A
34	N/A	AlexNet, ResNet, DenseNe, AML, SAGP, MAMC, GLPO-Net	P, R, F1	F1 – up to 97.5%	Keras
35	Rotation, horizontal flip, vertical flip, resizing	YOLOv2, YOLOv3, and YOLOv5	IoU, P, R, mAP	mAP are 92%, 97%, 94%	TensorFlow, Keras
36	Rotation at an angle of 90°, flipping left, right, up, and down	U-Net, SegNet, and DeepLabv3+	A, DSC	A are 89.5% and 67.3% for U-Net, 74.69% and 49.5% for SegNet, and 89.13% and	TensorFlow

				69.7% for DeepLabv3+	
37	N/A	ImageRatio, ImageRegr, DPCA, CVA, SSIM, FCN, Siamese network, our model E2	OA, F1, *k*	OA – 97.46%, F1 – 95.62%, *k* – 93.83%	TensorFlow
38	Horizontal flipping, random rotation by +30◦/−30◦, rescaling factor set to 3.92 · 10−3, zoom between 70% and 130%, and percentage of the image size to width and height shift at 30%	LSTM	P, R, F1, A	P is up to 85.30%	N/A
39	N/A	Multichannel Fusion CNN Based on Scattering Mechanism	OA, AA	OA – 95.83% and 98.15%, AA – 96.02% and 95.8%	N/A
40	N/A	GCK, MOR-KMM, 2DCNN, 3DCNN, SaSeLSTM, LWCNN-RAW, LWCNN-PCA, and lightweight CNN (LWCNN)	OA, AA, *k*	OA – 74.78%, 82.3%, 88.61; AA – 84.85%, 87.27%, 93.77%; *k* – 0.72, 0.78, 0.87 for IP	N/A
41	Random changes to the RGB channels of the original images and random vertical and horizontal flips	U-Net-like, CNN, AdaBoost, GaussianNB, KMM, Random Forest, and QDA	OA, F1, IoU	OA is up to 89%	Keras
42	Augmentation: Illumination, shadow, Hue change (summer), Hue change (early winter), Haze, snow; with multiple environmental conditions: summer w/good illumination; summer w/shadow; winter w/snow; early winter w/haze; summer w/dark	YOLOv3, CycledGAN,	P, R, mAP, F1	F1 are 0.59, 0.7, and 0.7 to 0.93, 0.94, and 0.89	N/A

	illumination.				
43	Searching similar samples of different window sizes, optimal selection of test samples after DA	PCANet with designed an effective structural feature extraction method (multi structure feature fusion, MSFF), MLR /SVM classification	AA, OA, *k*	AA is up to 99.89%	N/A
44	Cropping a large image into small patches	DL-EOBIA and a recently proposed Teacher-Student semi-supervised learning (SSL) approach (based on U-Net and U-Net++ networks)	P, R, OA, F1	OA – up to 85%, F1 – up to 84%	PyTorch, Scikit-learn, NumPy, Rasterio
45	Removing columns/rows of pixels at the sides of images, scaling, rotation, translation, horizontal and vertical shear	Mask R-CNN	P, R, F1, OA	F1 is from 95% to 98%	TensorFlow, Keras
46	Gaussian blurring, horizontal flip, vertical flip, rotation, and resizing	VGG16 and Wide ResNet50	OA	99.17%	PyTorch
47	Cropping a large image into small patches 27 × 27 pixels	U-net	F1, mAP, P, R	F1 – 0.73 and 0.59, mAP – 0.71 and 0.63	TensorFlow, Keras
48	A genetic algorithm as neuroevolution of augmenting topologies (NEAT)	SVM, PLS, Gradient boosting, RF, and NEAT	MAPE	31.75%	Scikit-learn
49	Implementing simple alterations, including cropping (reducing columns/rows of pixel value just at edges of images), scalability, inversion, transcription, horizontal, and vertical compressive	Mask Regional-CNN (inspired on ResNet50)	A, F1, R	F1 is from 95% to 98%	PyTorch

50	Horizontal flip, vertical flip, affine rotation, affine scaling, edge detection, and rotation with random value from −45° to 45° and scale value from 0.5 to 1.5	Proposed methods based on Mask R-CNN	P, R, IoU	mAP is 83.8%	N/A
51	Cropping a large image into small patches, rotating, flipping up and down, flipping left and right, brightening, contrast adjusting, chroma adjusting, and sharpening	FCN, SegNet, U-Net, U-Net-attention, AUD, and LodgeNet	P, R, F1, IoU, OA	OA is up to 97.3%	TensorFlow, Keras
52	Bayesian optimisation algorithms were utilised to select the optimal noise parameters of Gaussian, speckle, Poisson, and salt-and-pepper noise to generate new noisy images	GoogleNet, ResNet18, ResNet50, ShuffleNet, MobileNetv2, and DenseNet201	S, P, R, F1	AA – 99.5% and F1 – 100% (ResNet50)	Matlab, DL toolbox 2022b
53	Cut-and-paste method to simulate a more realistic scenario	YOLOV3	mAP	95%	N/A
54	Generating patches using the point-marginal method	CNN model developed by MathWorks	S, P, R, F1, A	S of 53%, P of 92%, and F1 of 67%	N/A
55	Rotating instances by a random angle between 0 and180°, transforming instances with a random size factor ranging between 0.6 and 1.2, and changing digital values for hue and	Mask R-CNN	mAP	mAP up to 83%	TensorFlow

	saturation of instances by 0–10% GAN framework with adapted discriminator augmentation StyleGAN-ADA				
56	Rotation, horizontal and vertical shift, and horizontal flip	AlexNet, VGG19, ResNet50, ARCNet, ICEL, MSCP, New one	OA	OA is up to 87.67% and 88.65% on new method	N/A
57	The whole dataset was divided into 3,000 super pixels based on turbopixels algorithms	EDb-CNN method based on ensemble learning and superpixels algorithms	OA, *k*	CA is up to 95.21% and 90.65%	TensorFlow
58	N/A	New sample 16-layer CNN, Bow, SSCBoW, FDDL, COPD, T-CNN, RICNN, Faster-RCNN, SSD, YOLOv3, RetinaNet, SCRDet, MLFF, and Few-shot (10-shot)	mAP	68.9%	N/A
59	Cropping a large image into small patches	Semantic segmentation regression network (SSRNet)	P, R, F1, A, R^2, RMSE	A, R^2, RMSE are 0.980, 0.996, 9.437	TensorFlow
60	N/A	A novel residual spatial attention kernel generation network (RSAKGN)	OA, AA, *k*	OA – up to 94.82±0.47, 98.48±0.32, 98.57±0.37	N/A
61	Generation of multiple views from the same sample and their consideration as similar pairs, while views derived from different samples are treated as dissimilar ones	SVM, CDCNN, SSUN, SSRN, HResNet, TSVM, CEGCN, 3DCAE, DFSL, DMVL, and S2FL	OA, AA, *k*	OA up to 97.67%	N/A
62	DA	U-net	P, F1, *k*	P – 99.20%, F1 – 96.66%, *k* – 0.91	N/A
63	N/A	CNN, CRNN, local features and a	OA, *k*	OA – up to 90.32%, *k* –	TensorFlow

		convolutional neural network (LF-CNN), k-nearest neighbour (KNN), LSTM		up to 0. 8792	
64	N/A	CNN+RGB, CNN+MS, MAML+CNN+RGB	A	Up to 99.53%	Matlab DL toolbox
65	Cropping into patches, random flipping, rotation by 20°, and cropping	DeepLab v3+, support vector classifier, Random Forest	A, IoU, F1	IoU of 0.77 and 0.90	PyTorch, TensorFlow
66	Element geometric transformation and GAN-based texture synthesis	(CNN)-ALEX-NET, VGG-NET, and RES-NET, alexNet	A	Up to 100%	Pytorch
67	Mosaic DA, adaptive anchor frame calculation, and adaptive image scaling	YOLOv5s, YOLOv5s + CBAM, YOLOv5s + SPPFP, YOLOv5s + BiFPN, YOLOv5s + VSP, YOLOv5s + VSP + CBAM, YOLOv5s + VSP + CBAM + SPPFP, YOLOv5s + VSP + CBAM + SPPFP + BiFPN	P, R, AP, mAP	mAP – up to 82.1%	PyTorch
68	N/A	Res-3D-CNN, M-HybridSN, AD-HybridSN, DFFN, MCNN-CP, MSSFN	OA, AA	OA is up to 99.43% (MSSFN)	TensorFlow
69	Random resized crop, colour jitters and rand augments + TL	Transformer NN, EfficientNet B1 and ResNet50	P, R, F1	F1 – up to 100%	TensorFlow, Keras
70	Cropping a large image into small patches, translation, rotation and inversion to fully extract the feature points	Mask R-CNN	P, R, F1, *k*, OA, mAP	mAP – up to 90.39%	TensorFlow, Keras
71	Image selection, image fusion, band combinations, visual interpretation, sample cutting, Jeffries–Matusita	AlexNet, GoogLeNet, SqueezeNet, ResNet-18, and VGG16	CA	94.9%	Matlab

	distance separability calculation, sample balance, and augmentation				
72	N/A	Baseline, Baseline + hybrid pyramid feature fusion, Baseline + coordinate attention, and Proposed	OA and AA	OA – 84.58%, 89%, 97.26%, AA – 89.68%, 87.37%, and 97.8% for IP, PU, and SA	PyTorch
73	Rotation (90°, 180°, and 270°), mirroring diagonally, and adding salt and pepper noise + TL	New IEU-Net	OA, F1, IoU	OA, F1, IoU – 93.12%, 91.4%, 89.9%	TensorFlow
74	N/A	The method combines the similarity calculation method GDSSM and the DL method 1D-CNN (GDSSM-CNN)	AA	AA – 91.2	Keras
75	Amplitude Domain Multiplicative Filtering (ADMF) image processing is mainly aimed at image amplitude domain processing, the speckle noise in the radar imaging process covers a wide range in the frequency domain, but is generally within a small range in the amplitude domain	Baseline CNN, A-ConvNet, CAE-CNN, Meta-Baseline, Da-Net, CAE_HL_CNN, LW_CMDANet, Unnamed method, AG-MsPN, ARGN, ADMF-FCNN, ADMF-IFCNN	AP	88.95%	TensorFlow
76	Cropping into patches	PointNet, PointNet (MSG), PointNet (SSG), PointMLP, PointMLT-elite, PointConv, DGCNN, PCT	OA, P, R, F1, *k*	OA is up to 94.5%	PyTorch
77	Python Augmentor package 0.2.9: random rotation, flip, random blur, random brightness	YOLOv5, YOLOR, DETR, Faster R-CNN	P, R, IoU, mAP	mAP with 50 and 95–95%, 92%, 93%, and 79%	PyTorch

78	N/A	Faster-RCNN	P, F1, R	P – 0.6845, F1 – 0.7993, R – 0.8236	TensorFlow
79	N/A	YOLO	P, R, F1	F1 – 91.05%	N/A
80	Mosaic method, where our images were integrated by random scaling, random clipping, and random arrangement; Methods for image down-sampling with Gaussian filter	Faster-RCNN, FCOS, and YOLOv5	P, R, RMSE	P – 0.822, R – 0.894, RMSE – 0.088	N/A